CHAPTER 9

Two-phase microfluidics, heat and mass transport in direct methanol fuel cells

G. Lu & C.-Y. Wang
Department of Mechanical Engineering and Electrochemical Engine Center (ECEC), The Pennsylvania State University, USA.

Abstract

This chapter provides an overview of the latest developments in direct methanol fuel cell (DMFC) technology. We begin by describing major technological challenges that DMFCs presently face for portable power, and demonstrate that the fundamental transport processes of methanol, water and heat, along with methanol oxidation kinetics, hold the key to successfully address these challenges. We then describe complementary experimental and modeling work to elucidate the critical transport phenomena, including two-phase microfluidics, heat and mass transport. We explain how the better understanding of these basic transport phenomena leads to a paradigm shift in the design of portable DMFCs, and show experimental evidence of surprisingly low methanol and water crossover through a very thin membrane, Nafion®112. Fuel efficiency resulting from low methanol crossover reaches 78% and net water transport coefficient through the membrane is found to be less than unity. These salient characteristics will enable highly concentrated methanol to be used directly and hence lead to much higher energy density for next-generation portable DMFCs. Finally, the latest research on micro-DMFCs is reviewed.

1 Introduction

A direct methanol fuel cell (DMFC) is an electrochemical cell that generates electricity based on the oxidation of methanol and reduction of oxygen. Figure 1 illustrates the cell construction and operating principles of a DMFC. An aqueous methanol solution of low molarity acts as the reducing agent that traverses the anode flow field. Once inside the flow channel, the aqueous solution diffuses through the backing layer, comprised of carbon cloth or carbon paper. The backing

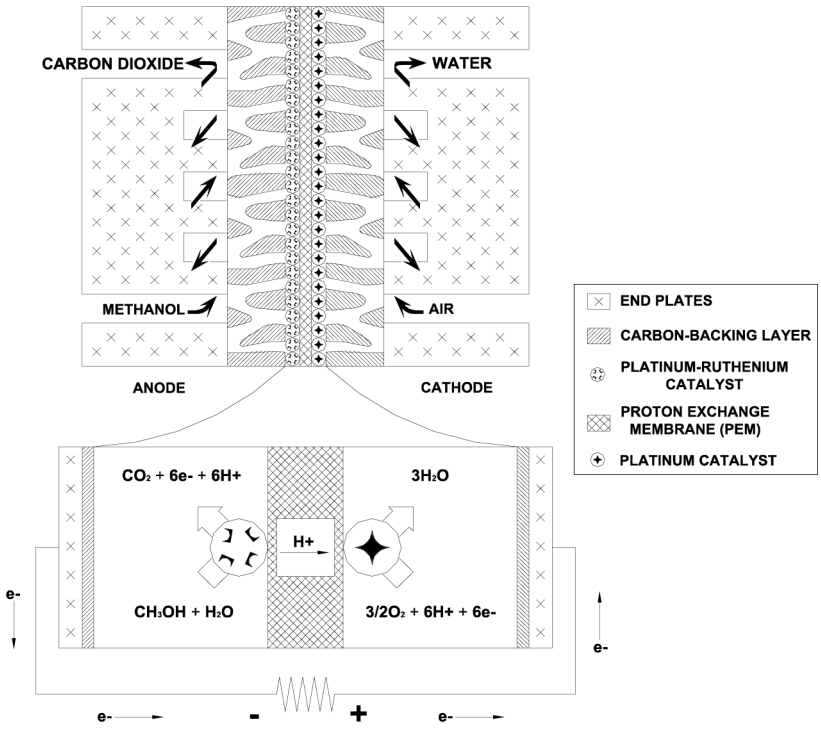

Figure 1: Operating schematic of a DMFC [1].

layer collects the current generated by the oxidation of aqueous methanol and transports it laterally to ribs in the current collector plate. The global oxidation reaction occurring at the platinum-ruthenium catalyst of the anode is given by:

$$CH_3OH + H_2O \rightarrow CO_2 + 6H^+ + 6e^-. \tag{1}$$

The carbon dioxide generated from the oxidation reaction emerges from the anode backing layer as bubbles and is removed via the flowing aqueous methanol solution.

Air is fed to the flow field on the cathode side. The oxygen in the air combines with the electrons and protons at the platinum catalyst sites to form water. The reduction reaction taking place on the cathode is given by:

$$\tfrac{3}{2}O_2 + 6H^+ + 6e^- \rightarrow 3H_2O. \tag{2}$$

These two electrochemical reactions are combined to form an overall cell reaction as:

$$CH_3OH + \tfrac{3}{2}O_2 \rightarrow CO_2 + 2H_2O. \tag{3}$$

Extensive work on DMFCs has been conducted by many groups, notably Halpert *et al.* [2] of Jet Propulsion Laboratory (JPL) and Giner, Inc, Baldauf and Preidel [3] of Siemens, Ren *et al.* [4] of Los Alamos National Laboratory (LANL), Scott and co-workers [5–7] of University of Newcastle upon Tyne, and Wang and co-workers [8–11] of the Pennsylvania State University. A comparative study of DMFC with H_2/air polymer electrolyte fuel cells (PEFC) was presented by the LANL group [4–12], demonstrating that a DMFC requires platinum-ruthenium and platinum loadings roughly five times higher to achieve power densities of 0.05 to 0.30 W/cm^2.

A number of extensive reviews have been published in recent years as worldwide DMFC research activities grew exponentially. Gottesfeld and Zawodzinski [13] briefly summarized research at Los Alamos intended for transportation application, and pointed out areas for improvement if DMFC technology is to become a serious power plant candidate for transportation. Among these challenges, reducing catalyst loading to compete with reformed/air fuel cells is perhaps the greatest, and presents a difficult task for the foreseeable future. In a later book chapter, Gottesfeld and Wilson [12] discussed perspectives on DMFC for portable applications. Lamy *et al.* [14] provided an in-depth review of DMFC fundamentals, including the reaction mechanisms of methanol oxidation, use of various binary and ternary electrocatalysts, effects of electrode structure and composition on the activity of methanol oxidation, and development of proton conducting membranes with low methanol crossover. It was projected that DMFCs will be commercialized as portable power sources before the year 2010 and that a quantum jump in technology will occur, making it possible to drive DMFC-powered vehicles ten years thereafter. Arico *et al.* [15] reviewed recent advances in DMFC from both fundamental and technological aspects. The fundamental aspects concerned electrocatalysis of methanol oxidation and oxygen reduction in the presence of methanol crossover, and the technological aspects focused upon the proton conducting membranes, as well as MEA fabrication techniques. Neergat *et al.* [16] provided an excellent review of new materials for DMFC, including novel proton conducting membranes and electrocatalysts. Narayanan *et al.* [17] and Muller *et al.* [18] discussed, in detail, the paramount importance of water balance to the portable DMFC system.

As expected, a DMFC exhibits lower power densities than that of a H_2/air PEFC, which at present requires anode and cathode platinum loadings of less than 1 mg/cm^2 to achieve power densities of 0.6 to 0.7 W/cm^2. However, the DMFC has the advantages of easier fuel storage, no need for humidification, and simpler design. Thus, DMFC is presently considered a leading contender for portable power application. To compete with lithium-ion batteries, the first and foremost property of a portable DMFC system must be higher energy density in Wh/L. This requirement entails overcoming four key technical challenges: (1) low rate of methanol oxidation kinetics on the anode, (2) methanol crossover through the polymer membrane, (3) water management, and (4) heat management.

The present chapter deals with the fundamental transport processes of methanol, water and heat underlying DMFCs. The basic transport phenomena, along with electrochemical kinetics, are critical to addressing the four technical challenges outlined above. Section 2 summarizes the thermodynamics and electrochemical

kinetics of DMFCs. Section 3 discusses the two-phase micofluidic phenomena in the DMFC anode and cathode, respectively, based on experimental observations. Section 4 describes mass transport phenomena in DMFC with focus on methanol crossover and water management issues. Section 5 treats heat transfer in DMFC and its coupling with water transport. Section 6 presents a review of mathematical modeling and experimental diagnostic techniques presently under active research. Finally, in Section 7 we present an exciting application of DMFC technology to power microsystems.

2 Fundamentals of DMFC

2.1 Cell components and polarization curve

The heart of a DMFC is a membrane-electrode assembly (MEA) formed by sandwiching a perfluorosulfonic acid (PFSA) membrane between an anode and a cathode. Upon hydration, the polymer electrolyte exhibits good proton conductivity. On either side of this membrane are anode and cathode, also called catalyst layers, typically containing Pt-Ru on the anode side and Pt supported on carbon on the cathode side. Here the half-cell reactions described in eqns (1) and (2) are catalyzed. On the outside of the MEA, backing layers made of non-woven carbon paper or woven carbon cloth, shown in Fig. 2, are placed to fulfill several functions. The primary purpose of a backing layer is to provide lateral current collection from the catalyst layer to the ribs as well as optimized gas distribution to the catalyst layer through diffusion. It must also facilitate the transport of water out of the catalyst layer. This latter function is usually accomplished by adding a coating of hydrophobic polymer, polytetrafluoroethylene (PTFE), to the backing layer. The hydrophobic character of the polymer allows the excess water in the cathode catalyst layer to be expelled from the cell by the gas flowing inside the channels, thereby alleviating flooding.

The microstructure of the catalyst layer is of paramount importance for the kinetics of an electrochemical reaction and species diffusion. Figure 3 shows scanning

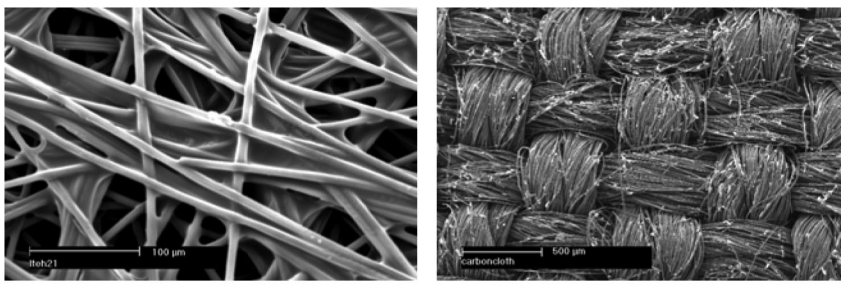

(a) (b)

Figure 2: SEM micrographs of (a) carbon paper and (b) carbon cloth.

electron microscopy (SEM) images of such microstructures of the DMFC anode and cathode, respectively, where high surface areas for electrochemical reactions are clearly visible.

A cross-sectional SEM of a MEA segment consisting of a backing layer, a microporous layer (MPL) and a catalyst layer, is displayed in Fig. 4 [9]. The MPL, with an average thickness of 30 μm, overlays a carbon paper backing layer. The anode catalyst layer of about 20 μm in thickness covers the MPL. In the anode, this MPL provides much resistance to methanol transport from the feed to the catalyst sites, thus reducing the amount of methanol crossover. In the cathode, the MPL helps alleviate cathode flooding by liquid water [19].

Figure 5 displays a voltage vs. current density polarization curve of a typical DMFC. The thermodynamic equilibrium cell potential for a DMFC, as calculated in Section 2.2, is approximately equal to 1.21 V. However, the actual open circuit voltage in DMFCs is much lower than this thermodynamic value, largely due to

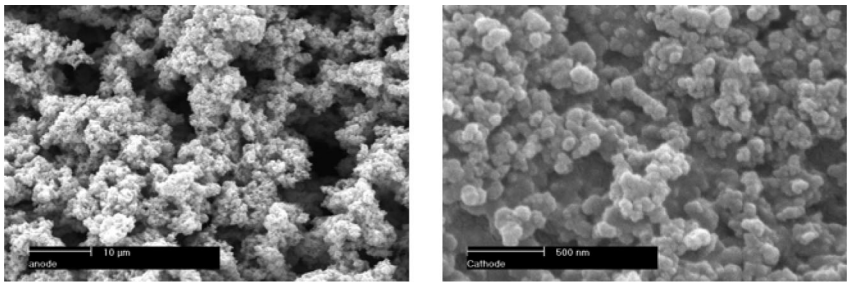

(a) anode (b) cathode

Figure 3: SEM images of electrodes.

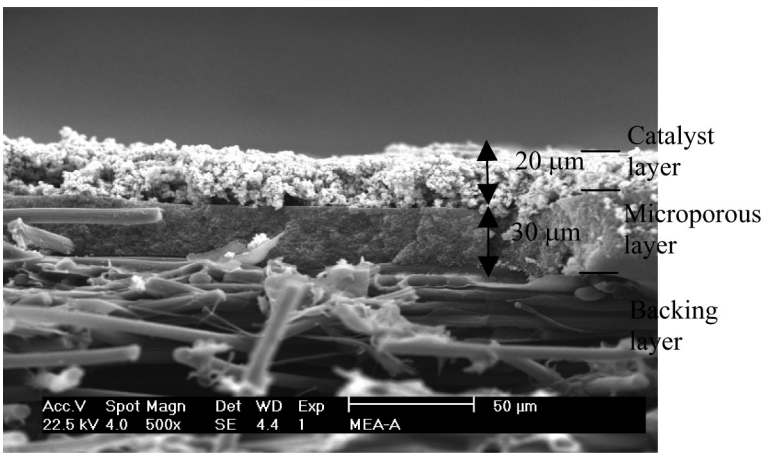

Figure 4: Cross-sectional SEM micrograph of backing layer, microporous layer, and catalyst layer.

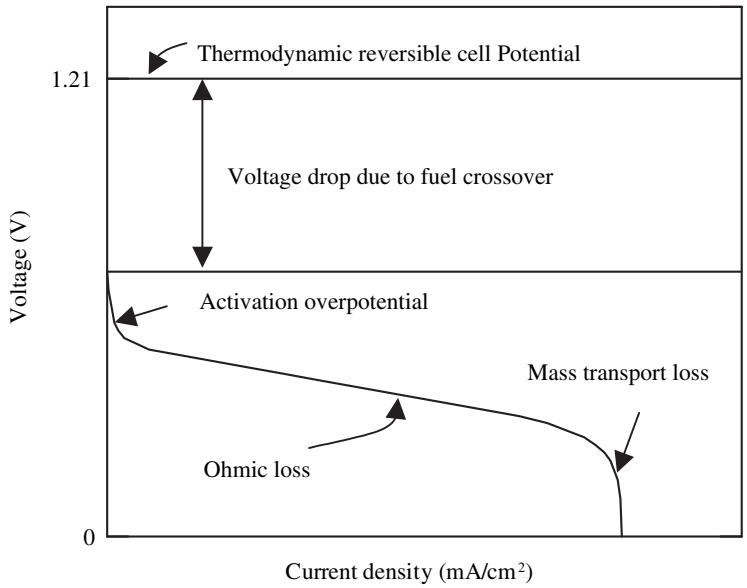

Figure 5: Schematic of DMFC polarization curve.

fuel crossover. Methanol crossover is an important topic in DMFCs and thus will be fully elaborated in Section 4.1. On closed circuit, the polarization curve can be categorized into three distinctive regions: kinetic control, ohmic control, and mass transport control. The kinetic control region of DMFC is dictated by slow methanol oxidation kinetics at the anode as well as oxygen reduction kinetics at the cathode. In this region a DMFC suffers the voltage loss second only to the low open circuit voltage caused by methanol crossover. More detailed discussion of this aspect is provided in Section 2.3. The area where cell voltage decreases nearly linearly in the polarization curve is recognized as the ohmic control region. For a DMFC where the polymer electrolyte is usually well hydrated, the voltage loss in this section is minimal. The last portion is referred to as the mass transport control region, whereby either methanol transport on the anode side results in a mass transport limiting current, or the oxygen supply due to depletion and/or cathode flooding becomes a limiting step. The cell voltage drops drastically in the mass transport control region.

2.2 Thermodynamics

The thermodynamic equilibrium potential of a fuel cell can be calculated from:

$$\Delta E = -\frac{\Delta g}{nF} = -\frac{\Delta h - T\Delta s}{nF}. \tag{4}$$

Table 1: Thermodynamic data of fuel cell reactions (per mole of fuel) [20].

Reaction	T (K)	Δg (kJ/kg)	Δh (kJ/kg)	Δs (kJ/kg K)	n	ΔE (V)	η_{rev}
PEFC	298	−237	−285	−162	2	1.23	0.83
DMFC	298	−704	−727	−77	6	1.21	0.97

PEFC: $H_2 + \frac{1}{2}O_2 \rightarrow H_2O$; DMFC: $CH_3OH + \frac{3}{2}O_2 \rightarrow CO_2 + 2H_2O$.

Table 1 lists thermodynamic data of common fuel cell reactions at 25 °C and 1 atm. For the liquid-feed DMFC, $n = 6$ and the thermodynamic cell potential is 1.21 V, similar to that of the H_2/air PEFC.

The thermodynamic efficiency of a fuel cell is defined as the ratio of maximum possible electrical work to the total chemical energy, i.e.:

$$\eta_{\text{rev}} = \frac{\Delta g}{\Delta h} = \frac{nF\,\Delta E}{-\Delta h}. \tag{5}$$

As shown in Table 1, the theoretical thermodynamic efficiency of DMFC reaches 97% at 25 °C.

The practical energy efficiency, however, is much lower after accounting for voltage and fuel losses. The voltaic efficiency is defined as the ratio of the actual electric work to the maximum possible work, with the former given by:

$$W_{\text{act}} = -nFV_{\text{cell}}, \tag{6}$$

where V_{cell} is the cell voltage at a current of I. Hence the voltaic efficiency can be written as:

$$\eta_{\text{voltaic}} = \frac{W_{\text{act}}}{W_{\text{max}}} = \frac{-nFV_{\text{cell}}}{\Delta g} = \frac{-nFV_{\text{cell}}}{-nF\,\Delta E} = \frac{V_{\text{cell}}}{\Delta E}. \tag{7}$$

For example, if the cell is running at 0.4 V, then the voltaic efficiency is only 33%. This low efficiency is caused by substantial overpotentials existed in both the anode and cathode of a DMFC.

In a DMFC, there is also fuel efficiency due to methanol crossover defined as:

$$\eta_{\text{fuel}} = \frac{I}{I + I_{x\,\text{over}}}, \tag{8}$$

where $I_{x\,\text{over}}$ is an equivalent current density caused by methanol crossover under the operating current density of I.

The total energy efficiency of DMFC is therefore given by:

$$\eta = \eta_{\text{rev}}\eta_{\text{voltaic}}\eta_{\text{fuel}}. \tag{9}$$

Suppose that the fuel efficiency, η_{fuel}, in a DMFC is 80%, the total energy efficiency becomes $\eta = 97\% \times 33\% \times 80\% = 25.6\%$ with cell voltage of 0.4 V.

In comparison, for a PEFC $\eta = 83\% \times 0.7/1.23 = 40.5\%$ with the cell voltage of 0.7 V. The energy efficiency of the PEFC is relatively higher owing largely to its negligibly small fuel crossover and overpotential for hydrogen oxidation on the anode. It is evident from eqn (6) that in order to achieve higher energy-conversion efficiency, one must control methanol crossover so as to maintain high fuel efficiency (e.g. >80%). In addition, it is desirable to operate DMFCs at higher voltages. Thus, high-voltage performance is a high priority for portable DMFC development.

Waste heat produced in the DMFC can thus be expressed as:

$$Q = \frac{IV_{\text{cell}}}{\eta} - IV_{\text{cell}} = IV_{\text{cell}}(1/\eta - 1). \tag{10}$$

By substituting the definition of the total energy efficiency, another expression of heat generation results:

$$Q = (-\Delta h)\frac{I + I_{x\,\text{over}}}{nF} - IV_{\text{cell}}, \tag{11}$$

where the first term on the right hand side represents the chemical energy of methanol consumed for power generation and by crossover, while the second term stands for the electric energy generated.

2.3 Methanol oxidation and oxygen reduction kinetics

Combined with methanol crossover, slow anode kinetics lead to power density in a DMFC that is three to four times lower than that of a hydrogen fuel cell. Much work has been focused on the anodic oxidation of methanol [21]. A multi-step mechanism of electrocatalytic oxidation of methanol at the anode was postulated [22, 23]. Different anode catalyst structures of Pt-Ru were developed [24] and several anode catalysts other than Pt-Ru were explored [25–27]. Additionally, the effects of the anode electrochemical reaction on cell performance were experimentally studied [28–30]. Lamy *et al.* [14] and Arico *et al.* [15] provided extensive reviews of the most recent work on electro-catalysis. More active catalysts for methanol oxidation would enable a certain power density to be realized at higher cell voltage, and hence directly impact the energy efficiency of the cell, which translates to the energy density if the amount of fuel carried by a DMFC system is fixed.

The activation overpotential of methanol oxidation reaction (MOR) can be described by Tafel kinetics of the following form:

$$\eta_a = b_a \log\left(\frac{I}{I_{0,a}}\right), \tag{12}$$

where b_a and $I_{o,a}$ are the Tafel slope and exchange current density of MOR, respectively. A convenient method to characterize anode activation polarization uses a MeOH anode vs. H_2 cathode cell as proposed by Ren *et al.* [28], to be discussed in more detail in Section 7.

The oxygen reduction reaction (ORR) on the DMFC cathode is similarly slow, causing a high cathode overpotential. Thus, a Tafel expression is usually used to describe ORR kinetics as follows:

$$\eta_c = b_c \log\left(\frac{I}{I_{o,c}}\right), \tag{13}$$

where the Tafel slope for ORR is around 70 mV/decade in the absence of methanol oxidation. However, in DMFCs, ORR takes place simultaneously with oxidation of crossover methanol, and consequently b_c for a DMFC becomes greater than that for a H_2/air PEFC.

3 Two-phase flow phenomena

3.1 Bubble dynamics in anode

On the anode side, carbon dioxide is produced as a result of MOR. If CO_2 bubbles cannot be removed efficiently from the surface of the backing layer, they remain, covering the backing surface and hence decreasing the effective mass transfer area. In addition, flow blockage results, particularly in channels of small dimensions as required in micro or compact portable fuel cells with maximum volumetric power and energy densities. Therefore, gas management on the anode side is an important issue in DMFC design. Argyropoulos *et al.* [5, 31] was perhaps among the first to observe the two-phase flow pattern in the anode channel under various operating conditions. This flow visualization on the anode side yields valuable understanding of bubble dynamics in a DMFC. This study was, however, undertaken under low cell performance. Most recently, Lu and Wang [32] developed an improved transparent DMFC to visualize bubble dynamics on the anode side and liquid droplet (and flooding) dynamics on the cathode. This latest study is described in detail in the next two subsections.

3.1.1 Flow visualization

Figure 6 displays a diagram of the experimental setup, which consists of an electronic load system to characterize polarization behaviors of the fuel cell, a peristaltic pump to deliver the liquid fuel, an electric heater with temperature controller, pressure relief valves, flow meters and pressure gauges. A Sony digital video camera recorder was used in experiments for flow visualization, and still pictures were captured according to the time sequence when the movie was edited offline. Also, a Nikon N70 camera with a micro-Nikkor lens (60 mm f/2.8D) was utilized to obtain clear pictures of small-size objects.

Figure 7 shows a picture of the transparent fuel cell. The cell was constructed of a pair of stainless steel plates mated with a polycarbonate plate. A total of eight parallel flow channels (1.92 mm width, 1.5 mm depth, 1 mm rib width) were machined through the stainless steel plate to form an active area of approximately 5 cm^2. The surface of the stainless steel plate contacting the MEA was coated with 30 nm Cr and 300 nm Au to minimize contact resistance. A transparent polycarbonate plate

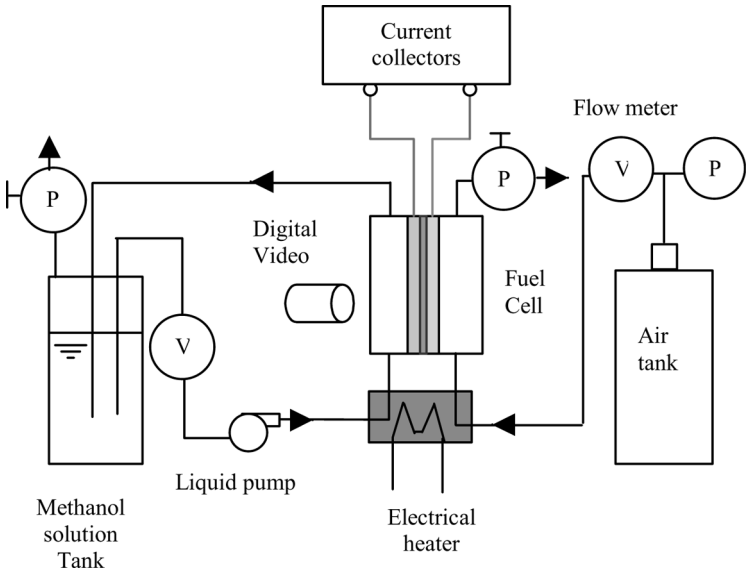

Figure 6: Experimental setup for flow visualization.

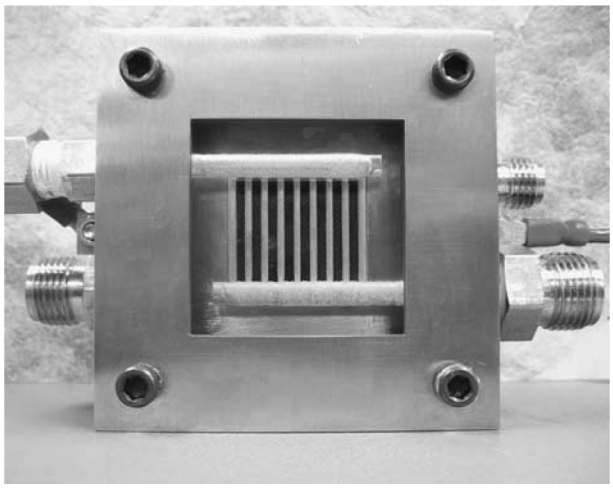

Figure 7: Photo of the transparent fuel cell.

covered the stainless steel plate, forming a window to allow direct observation of flow behaviors. The polycarbonate plate was concave in design, while the stainless steel plate had a matching convex pattern. This unique design avoided flow leakage between neighboring parallel channels. Cell inlet and outlet manifolds were also machined in the polycarbonate plates.

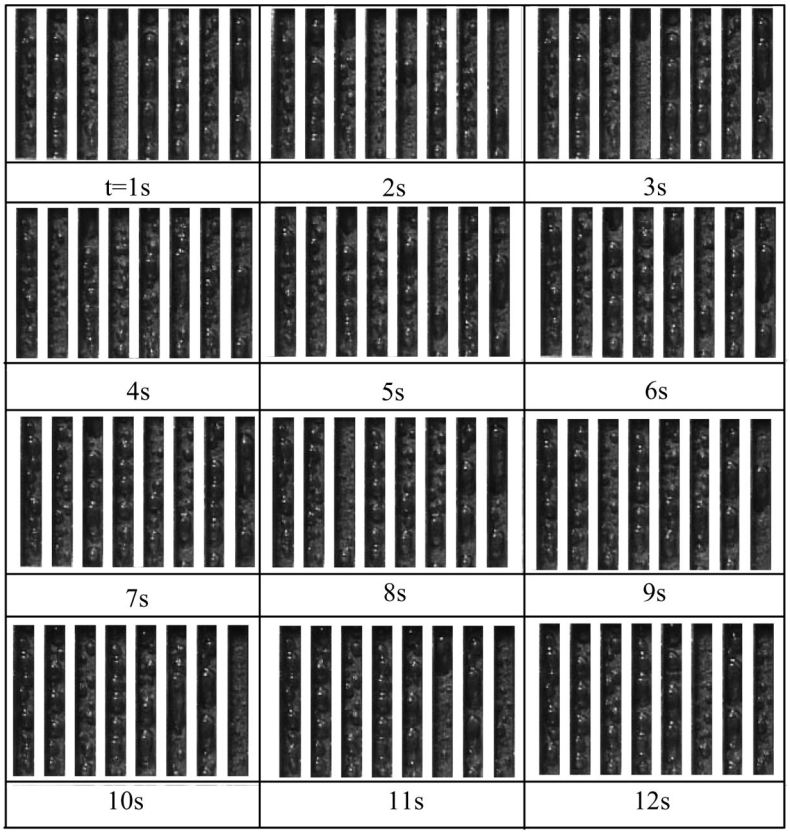

Figure 8: Images of bubble dynamics in the DMFC anode using a MEA with carbon paper as backing layer for 2 M MeOH feed and non-humidified air at 100 mA/cm^2 and 85°C.

Figure 8 shows a sequence of images at various times for an MEA with hydrophobic carbon paper as the backing layer at the feed temperature of 85 °C and the current density of 100 mA/cm^2. The images, one second apart, were captured from the movie, with time resolution 1/30 second. In addition, the time of the first image was chosen arbitrarily due to the fact that two-phase flow is a regularly periodic event and the cell was operated at steady-state. As shown in Fig. 8, the CO_2 bubbles nucleate at certain locations and form large and discrete gas slugs in the channel. The CO_2 bubbles are large in size ($\sim$2 mm) and confined by the channel dimensions, elongated in shape, and distributed discretely on the backing layer along the anode channel. This bubble flow is commonly categorized as Taylor bubbles. The bubble motion is governed by the momentum of liquid flow, the force of buoyancy on the bubble, and the surface tension between bubbles and substrate. It can be seen from Fig. 8 that the bubbles are held on the carbon paper by strong surface tension until they grow into larger slugs for detachment, clearly indicative of the dominant

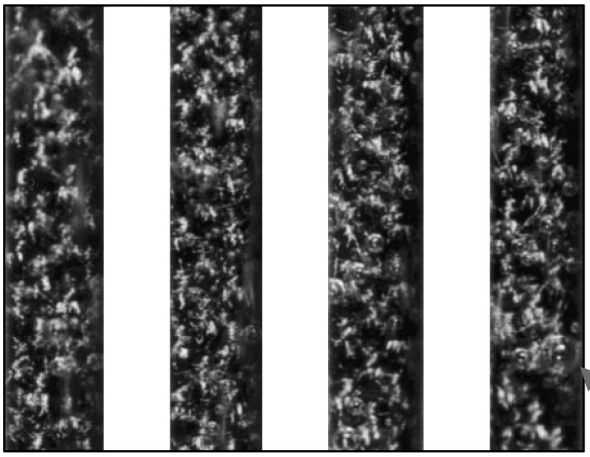

Figure 9: Bubble behavior on the anode side using hydrophilic carbon cloth for 1 M MeOH feed and non-humidified air at 100 mA/cm^2 and 85 °C.

effect of surface tension in bubble dynamics in DMFC. Once the bubbles grow to a sufficient size, they detach and sweep along the backing surface in the channel. This sweeping process clears all small bubbles pre-existing on the backing surface, making new bubbles grow from the smallest size to full detachment diameter. As a result, the two-phase flow becomes regularly intermittent. The flow pattern on the MEA with carbon paper is characterized as bubble flow or slug flow, depending on the accumulation of the bubbles.

Figure 9 shows the bubble patterns on the MEA with hydrophilic carbon cloth also at the feed temperature of 85 °C. Since the carbon cloth has a much rougher surface, it is challenging to capture sharp still pictures due to light deflection, although the two-phase flow could be observed clearly in the experiments and movies. Alternatively, a Nikon N70 camera with a micro-Nikkor lens was employed for still photos. It is seen that the CO_2 bubbles are produced more uniformly and with smaller size (∼0.5 mm) from the hydrophilic carbon cloth. Therefore, the flow on the MEA with carbon cloth is characterized as a bubble flow.

The differences in bubble behaviors between hydrophobic carbon paper and hydrophilic carbon cloth can be explained by considering the fundamental process of bubble growth. It is insightful to compare the differences in the pore structure of carbon paper and carbon cloth. Figure 2 shows SEM micrographs of these two substrates. Clearly, carbon cloth has more regularly distributed pores, whereas carbon paper is more of a random porous medium. This difference in the pore size distribution gives rise to the fact that CO_2 bubbles emerge more uniformly from the carbon cloth than carbon paper.

3.1.2 Bubble diameter and drift velocity

The bubble detachment diameter from the backing layer is strongly correlated with surface wettability. Consider a bubble growing and detaching from a single pore

of known diameter, d_p, and surface contact angle of θ. Assuming, as was indicated in experimental observations, that the bubble detachment process is dominated by buoyancy and surface tension effects, the force balance predicts that the diameter of the bubble at detachment, d_b, is [33]:

$$d_b = \left(\frac{4 d_p \sigma \sin\theta}{g(\rho_l - \rho_g)} \right)^{\frac{1}{3}}. \tag{14}$$

With the typical pore size of 10 μm for both carbon paper and carbon cloth [34], eqn (14) calculates the bubble detachment diameter of 0.68 mm for the hydrophobic carbon paper (e.g. $\theta = 100°$) and 0.38 mm for the hydrophilic carbon cloth (e.g. $\theta = 10°$). These theoretical estimates are consistent with experimental observations.

Once detached, bubbles stay spherical in shape due to strong surface tension. If these bubbles are smaller than the channel dimension, the bubble drift velocity through the liquid can be estimated from the correlation of the bubble rising velocity through an infinite, stagnant liquid as obtained from the balance between inertia and gravitational forces [35], i.e.:

$$u_b = \frac{d_b^2 g(\rho_l - \rho_g)}{12 \mu_l}. \tag{15}$$

3.1.3 Pressure drop

For the purpose of gross estimation, the two-phase frictional pressure drop through the anode channel of a DMFC may be approximated by assuming a homogenous flow. Usually, the two-phase flow in the DMFC anode is laminar as the flow rates of both phases are quite small. For a 50 cm^2 DMFC operated under typical conditions, the anode pressure drop is of the order of a few kPa.

3.2 Liquid water transport in cathode

The importance of flooding on the cathode side in H_2/air PEFCs has been emphasized in the literature [36–39]. Similarly, water management on the cathode in a DMFC was identified as a key issue [40]. A proper level of liquid water existing in the DMFC cathode helps to hydrate the polymer membrane, thus increasing the proton conductivity. However, severe flooding should be avoided so as to maintain the cathode performance.

3.2.1 Flooding in the cathode

In the cathode, water is produced by the oxygen reduction reaction as well as transported from the aqueous anode due to diffusion and electro-osmotic drag. Parameters governing liquid water formation and distribution in the cathode include the stoichiometry (or volumetric flow rate) of the inlet air, current density, cell temperature, and membrane water transport properties such as the diffusion coefficient and electro-osmotic drag coefficient.

Formally, the water flux arrived at the cathode by diffusion, electro-osmosis, and hydraulic permeation across the membrane can be expressed as [40]

$$j_m = -D\frac{\Delta C_{c-a}}{\delta_m} + n_d\frac{I}{F} - \frac{K_m}{\mu_l}\Delta P_{c-a}\frac{\rho_l}{M_{\mathrm{H_2O}}} = \alpha\frac{I}{F}. \tag{16}$$

Clearly, the three terms on the right hand side in eqn (16) represent three modes of water transport through the membrane, respectively. The molecular diffusion is driven by the concentration gradient. The electro-osmotic drag is proportional to the current density, and the permeation is driven by the hydraulic pressure difference. The net water flux through the membrane can be conveniently quantified by a net water transport coefficient, α, as defined in eqn (16). This important parameter dictates water management strategies in DMFC systems. It is a combined result of electro-osmotic drag, diffusion and convection through the membrane. For thick membranes like Nafion®117, α approaches the electro-osmotic drag coefficient as the other two modes of water transport are weakened with increasing membrane thickness.

The electro-osmotic drag coefficient n_d for Nafion electrolyte in contact with liquid water depends on the temperature [41], as shown in Fig. 10. The relation can also be fitted as:

$$n_d = 1.6767 + 0.0155\mathrm{T} + 8.9074 \times 10^{-5}\,\mathrm{T}^2, \tag{17}$$

where T is the cell temperature in °C.

The total rate of water transported to and produced at the cathode is given by:

$$j_{\mathrm{H_2O}} = \left(\alpha + \frac{1}{2}\right)\frac{I}{F}. \tag{18}$$

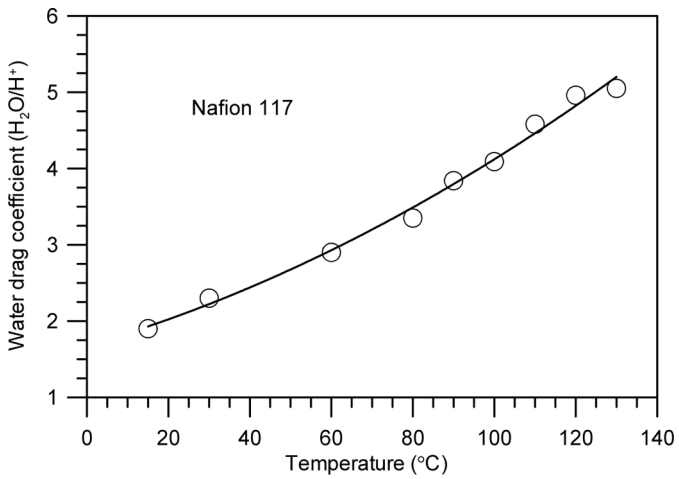

Figure 10: Water drag coefficient as a function of temperature [41].

At steady state, this must be balanced by the removal rate through cathode air flow. Suppose that completely dry air is fed into the cathode channel, its molar flow rate can be expressed as a function of air stoichiometry such that:

$$j_{air} = \frac{1}{0.21}\xi\frac{I}{4F}, \tag{19}$$

where ξ is the stoichiometry defined at the current density of I.

The depletion rate of oxygen due to the ORR is simply given by:

$$j_{O_2} = \frac{I}{4F}. \tag{20}$$

A simple water balance thus yields the relative humidity of air at the cathode exit as follows:

$$\begin{aligned} RH_{\text{exit}} = \frac{p_{H_2O}}{p_{\text{sat}}(T)} &= \frac{\frac{I}{F}\left(\frac{1}{2}+\alpha\right)}{\xi\frac{1}{0.21}\frac{I}{4F} - \frac{I}{4F} + \frac{I}{F}\left(\frac{1}{2}+\alpha\right)} \times \frac{p_{\text{total}}}{p_{\text{sat}}(T)} \\ &= \frac{1+2\alpha}{\frac{\xi}{0.42}+0.5+2\alpha} \times \frac{p_{\text{total}}}{p_{\text{sat}}(T)}. \end{aligned} \tag{21}$$

A critical air stoichiometry is obtained when the relative humidity $RH_{\text{exit}} = 100\%$, i.e.:

$$\xi_{\text{cri}} = 0.21\left[(2+4\alpha)\frac{p_{\text{total}}}{p_{\text{sat}}(T)} - (1+4\alpha)\right]. \tag{22}$$

This threshold stoichiometry represents the formation of liquid water and thus characterizes the state of cathode flooding. If the actual stoichiometry is smaller than that given in eqn (22), the cathode exhaust air will carry liquid water and hence cathode flooding likely occurs. On the other hand, if the actual air stoichiometry is higher, the cathode exhaust air is under-saturated. In this case, cathode flooding is avoided; however, there is too much water loss through evaporation in the case of large air flowrate. Recovery of water vapor in an external condenser proves to be a difficult task for a compact portable system. Hence, for portable DMFC systems, air stoichiometry ought to be designed to be smaller than the critical value given in eqn (22), implying at the same time that a small amount of cathode flooding is inevitable in portable systems.

3.2.2 Flooding visualization

Visualization on the cathode side is a useful diagnostic tool to understand the nature of flooding. Figure 11 displays an image of water drop formation on carbon paper treated with PTFE with non-humidified air preheated to 85 °C and fed at a volumetric flow rate of 68 mL/min using the transparent cell as shown in Fig. 7. The cell current density was 100 mA/cm^2. It is shown in Fig. 11 that water droplets are attached on the surface of the carbon paper due to its decreased hydrophilicity

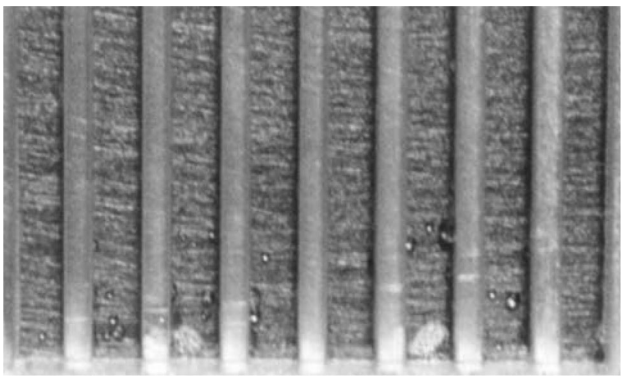

Figure 11: Water droplet formation at cathode using Toray carbon paper for 2 M MeOH feed and non-humidified air (68 mL/min and 1 psig) at 100 mA/cm^2 and 85 °C.

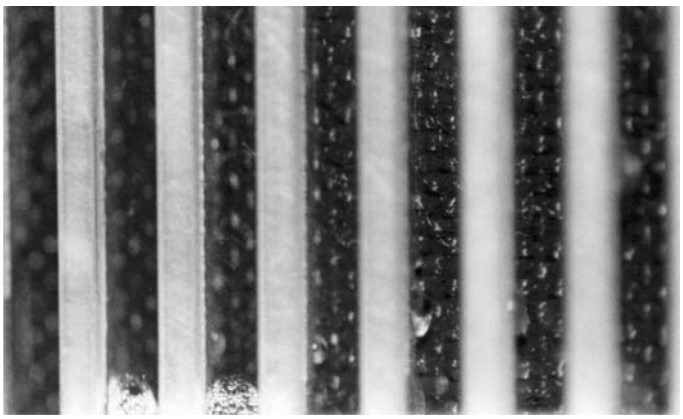

Figure 12: Cathode flooding on single-sided ELAT carbon cloth for 2 M MeOH feed and non-humidified air (161 mL/min and 1 psig) at 60 mA/cm^2 and 85 °C.

at elevated temperatures. It was observed that while the droplets grow slowly, the cell voltage drops gradually when the current density is fixed.

Figure 12 shows an image of flooding on the single-sided ELAT carbon cloth with non-humidified air preheated to 85 °C. It is seen from Fig. 12 that the surface of carbon cloth is nearly free of liquid droplets due to its higher hydrophobicity, but liquid droplets or 'sweating' can be found in contact corners between the stainless steel rib and carbon cloth. This is because the rib surface is rather hydrophilic. Interestingly, it appears that sweating inside corners between the ribs and carbon cloth gas diffusion layer occurs at a rather low current density of 60 mA/cm^2 and a high air flow rate of 161 mL/min. In comparison, no such sweating is seen

between the stainless steel ribs and carbon paper GDL at a higher current density of 100 mA/cm^2 and a lower airflow rate of 68 mL/min (see Fig. 11).

Much remains to be learned about the fundamental process of flooding occurrence and its relation with the backing layer material.

4 Mass transport phenomena

4.1 Methanol crossover

Methanol crossover occurs due to the inability of the commonly-used perfluorosulfonic acid (PFSA) membrane to prevent methanol from permeating its polymer structure. Diffusion and electro-osmotic drag are the prime driving forces for methanol transport through the polymer membrane and eventual reaction with platinum catalyst sites on the cathode, leading to a mixed potential on the cathode. This mixed potential on the cathode causes a decrease in cell voltage. Methanol reaching the cathode also results in decreased fuel efficiency, thus lowering the energy density of the system.

Methanol crossover in DMFC has been extensively studied both experimentally and theoretically. Narayanan *et al.* [42] and Ren *et al.* [43] measured the methanol crossover flux with different membrane thickness and showed that methanol crossover rate is inversely proportional to membrane thickness at a given cell current density, thus indicating that diffusion is dominant. In addition, Ren *et al.* [44] compared diffusion with electro-osmotic drag processes and demonstrated the importance of electro-osmotic drag in methanol transport through the membrane. In their analysis, methanol electro-osmotic drag is considered a convection effect and the diluted methanol moves with electro-osmotically dragged water molecules. Valdez and Narayanan [45] studied the temperature effects on methanol crossover and showed that the methanol crossover rate increases with cell temperature. Ravikumar and Shukla [30] operated a liquid-feed DMFC at an oxygen pressure of 4 bars and found that cell performance is greatly affected by methanol crossover at methanol feed concentrations greater than 2 M, and that this effect increases with increased operating temperature. Wang *et al.* [46] analyzed chemical composition of the cathode effluent of a DMFC using a mass spectrometer. They found that methanol crossing over the membrane is completely oxidized to CO_2 at the cathode in the presence of a Pt catalyst.

Additionally, the cathode potential is influenced by the mixed potential phenomenon due to simultaneous methanol oxidation and oxygen reduction as well as poisoning of Pt catalysts by methanol oxidation intermediates. Kauranen and Skou [47] presented a semi-empirical model to describe the methanol oxidation and oxygen reduction reactions on the cathode and concluded that the oxygen reduction current is reduced in the presence of methanol oxidation due to surface poisoning. Kuver and Vielstich [48] studied the dependence of crossover on reaction conditions, such as temperature and methanol concentration. Additionally, a cyclic voltammetry technique was presented which allows the evaluation of methanol

crossover in a fuel cell under operating conditions. Scott *et al.* [49] investigated the effect of cell temperature, air cathode pressure, fuel flow rate and methanol concentration on power performance. Gurau and Smotkin [50] used gas chromatography to measure crossover variation with temperature, fuel flow rate and concentration. Heinzel and Barragan [51] gave an extensive review of the state-of-the-art of methanol crossover in DMFC. Influence of methanol concentration, pressure, temperature, membrane thickness and catalyst morphology have been discussed.

Development of novel membranes with low methanol crossover would surely increase cell performance and fuel efficiency [14, 16, 52–54]. Alternatively, Wang and co-workers [9, 10, 55] proposed to modify the anode backing structure to mitigate methanol crossover. It was demonstrated that a compact microporous layer can be added in the anode backing to create an additional barrier to methanol transport, thereby reducing the rate of methanol crossing through the polymer membrane. Both practices to control methanol crossover by increasing mass transport resistance, either in the anode backing or in the membrane, can be mathematically formulated by a simple relation existing between the crossover current, I_c, and anode mass-transport limiting current, $I_{A,\mathrm{lim}}$. That is:

$$I_c = I_{c,oc}\left(1 - \frac{I}{I_{A,\mathrm{lim}}}\right), \tag{23}$$

where $I_{c,oc}$ is the crossover current at open circuit, and I the operating current. In the conventional approach using thick membranes with low methanol crossover, $I_{c,oc}$ is low and $I_{A,\mathrm{lim}}$ is set to be high. In contrast, setting up a barrier in the anode backing is essentially reducing the anode limiting current, $I_{A,\mathrm{lim}}$, and making $I_{c,oc}$ a significant fraction of $I_{A,\mathrm{lim}}$, about 50–80%. Two immediate advantages result from this latter cell design principle. One is that more concentrated fuel can be used thus leading to much higher energy density of the DMFC system. Lu *et al.* [10] successfully demonstrated the use of 8 M methanol solution as the anode feed, and Pan [55] most recently reported a DMFC operated with 10 M (or 30% by volume) methanol fuel solution. Secondly, this type of DMFC permits use of thin membranes such as Nafion 112, which greatly facilitates water back flow from the cathode to anode [10, 56], thus addressing another major challenge of portable DMFC to be discussed in the next subsection.

As an example, Fig. 13 shows the polarization curve of a DMFC design based on the above new concept and using a very thin membrane, Nafion 112. The cell was operated at an anode stoichiometry of 2 and a cathode stoichiometry of 4 at a current density of 150 mA/cm^2. It is evident from Fig. 13 that the mass transport limiting current density, $I_{A,\mathrm{lim}}$, in this cell is equal to 205 mA/cm^2. Figure 14 displays the polarization behavior of the cell when using humidified nitrogen in the cathode to obtain the crossover rate at the open circuit, which gives $I_{c,oc} = 157$ mA/cm^2. According to eqn (23), the crossover current at the operating current density of 150 mA/cm^2 is $I_c = 42$ mA/cm^2. Therefore, the fuel efficiency defined in eqn (8) reaches $150/(150+42) = 78\%$. This experiment provides direct evidence that it is possible to obtain very high fuel efficiency even when using a very thin membrane, Nafion 112, provided that the cell is well designed. Finally, this cell yields a power

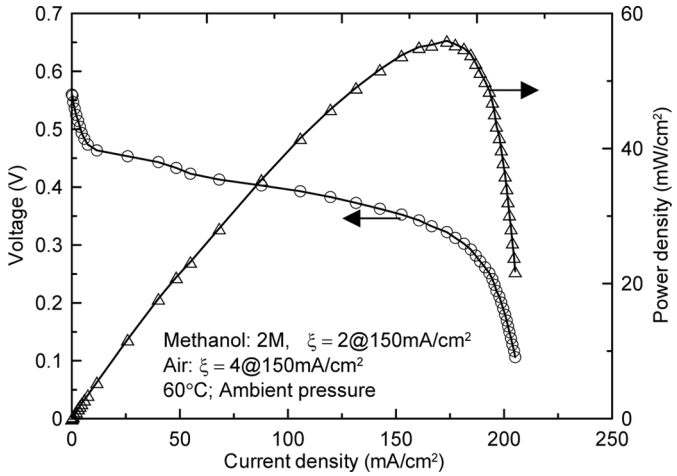

Figure 13: Polarization and power density curves for a DMFC designed for portable application.

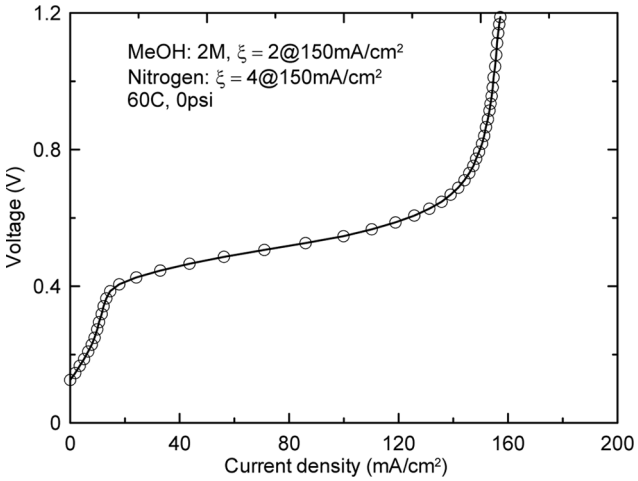

Figure 14: Measurement of methanol crossover current density at open circuit using humidified nitrogen in the cathode. The limiting current density signifies the crossover rate.

density of 56 mW/cm^2 at 60 °C under operating conditions eminently suited for portable systems.

4.2 Water management in portable DMFC systems

Water management emerges as a new significant challenge for portable DMFC systems. Constrained by the methanol crossover problem, the anode fuel solution

has been very dilute, meaning that a large amount of water needs to be carried in the system and therefore reduces the energy content of the fuel mixture. In addition, for each mole of methanol, one mole of water is needed for methanol oxidation at the anode and 2.5×6 moles of water are dragged through a thick membrane such as Nafion 117 towards the cathode, assuming that the electro-osmotic drag coefficient of water is equal to 2.5 water molecules per proton. This then causes 16 water molecules to be lost from the anode for every mole of methanol. Water in the anode must therefore be replenished. On the other hand, inside the cathode, there are 15 water molecules transported from the anode due to electro-osmosis and 3 additional water molecules produced by consuming six protons generated from oxidation of one methanol molecule. Presence of a large amount of water floods the cathode and reduces its performance. The difficult task of removing water from the cathode to avoid severe flooding and supplying water to the anode to make up water loss due to electro-osmotic drag through the membrane is referred to as innovative water management in a portable DMFC.

Traditionally, a high cathode gas flow rate (high stoichiometry) is employed to prevent flooding. This strategy not only increases parasitic power consumption but also removes excessive water from the fuel cell, making external water recovery more difficult; see the discussion in Section 3.2.1. How to minimize water removal from the cathode and subsequent recovery externally to replenish the anode without causing severe cathode flooding becomes an important engineering issue. A greater understanding and ability to tailor water flow in the cell is of fundamental interest for portable DMFC systems. This is an area where DMFC modeling plays an important role.

In the open literature, Blum *et al.* [57] proposed a concept of a water-neutral condition under which the anode does not need water supply and the cell maintains perfect water balance by losing exactly 2 moles of water per mole of methanol consumed. Apparently, this condition corresponds to $\alpha = -1/6$. Most recently, Peled *et al.* [56] reported experimental data with α being small and even negative at low current densities by using a nonporous proton-conducting membrane and oxygen at 3 bars as the oxidant. It was postulated that the convection effect induced by a hydraulic pressure differential across the membrane can offset the electro-osmotic drag, leading to α being much smaller than the electro-osmotic drag coefficient of approximately 3 at 60 °C.

Low-α DMFCs are highly desirable from the water management standpoint as the anode does not require an excessive amount of water and, in conjunction with the methanol transport barrier concept suggested in Section 4.1, it becomes possible to use highly concentrated methanol fuel at the anode. In addition, there is less or no need to recover water from the cathode exhaust, thus eliminating or reducing the condenser in a portable system. Based on our theory of liquid water transport in PEFCs [19, 58], we have designed a unique MEA structure which utilizes the microporous layer, as shown in Fig. 4, to build up the hydraulic pressure on the cathode side and which then uses a thin membrane (i.e. Nafion 112) to promote the water back flow under this hydraulic pressure difference. Such MEAs exhibit extraordinarily low α and hence are generally termed low-α MEA technology.

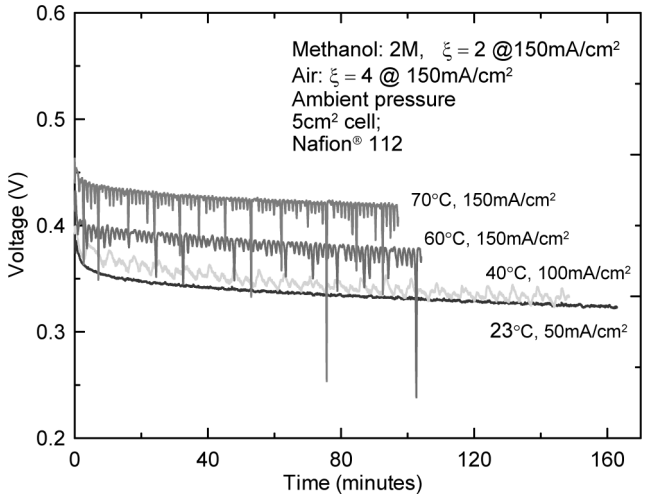

Figure 15: Evolutions in cell voltage during constant current loading to measure the net water transport coefficient α.

Figure 15 shows the evolution of cell voltage at constant current load in a series of experiments to measure the net water transport coefficient, α, at various temperatures using a moisture trap [59]. The steady-state power density reaches 16 mW/cm^2 at 23 °C, 33.3 mW/cm^2 at 40 °C and 56 mW/cm^2 at 60 °C, respectively. At low current densities, e.g. 50 mA/cm^2 at 23 °C and 100 mA/cm^2 at 40 °C, the cell voltages remain stable for an extended period of operation. While at a high current density such as 150 mA/cm^2 at 60 °C and 70 °C, the cell voltage occasionally experiences a sharp fluctuation once a slug of CO_2 gas produced by the large current density blocks the anode channels temporarily, causing a "short-lived" mass transport limitation on the anode side. Paying attention to gas management in the design of anode flowfield will likely remove this voltage oscillation.

Figure 16 displays the net water transport coefficient α measured at different temperatures. It is seen that α is only 0.05 at room temperature and α is equal to 0.64 at 60 °C for the air stoichiometry of 4 and methanol stoichiometry of 2. The significance of this set of experiments, shown in Figs 15 and 16, is the fact that commercially available Nafion membranes and MEA materials were used and the cell operated with ambient air without pressurization.

5 Heat transport

Thermal management in DMFCs is intimately tied to water and methanol transport processes. First, heat generation in DMFC is much higher than H_2/air PEFC due to a much lower energy efficiency (only 20–25% when the cell is operated between 0.3–0.4 V). That is, for a 20 W DMFC system, 60–80 W of waste heat is produced. The waste heat is typically removed from DMFC by liquid fuel on the anode side

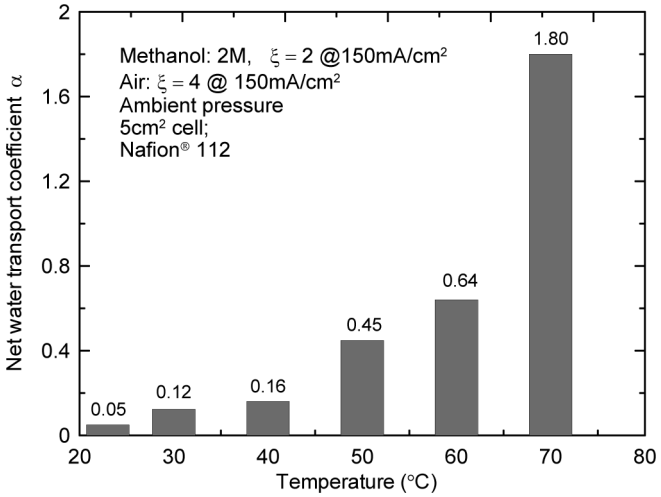

Figure 16: The net water transport coefficient α at different temperatures with constant flow rates of methanol and ambient air.

and by water evaporation on the cathode side. The latter also determines the amount of water loss from a DMFC and the load of water recovery by an external condenser. Therefore, while a higher cell temperature promotes the methanol oxidation reaction, it may not be practically feasible from the standpoint of water evaporation loss. Moreover, the higher cell temperature increases the methanol crossover rate, thereby reducing the fuel efficiency and the system energy density.

Argyropoulos *et al.* [60] present a one-dimensional thermal model for direct methanol fuel cell stacks. In this model, the variation of the temperature of the various components in the stack as well as the heat flow inside the system has been assessed. Dohle *et al.* [61] described the heat and power management of a direct methanol fuel cell by taking the power for auxiliary equipment into consideration. However, a heat flow analysis carried out for portable DMFC systems is absent in the open literature.

The total waste heat produced from DMFC reactions has been derived in Section 2.2, i.e. eqn (11). In addition, a heat sink term exists due to liquid water evaporating into the gas phase in the cathode. This can be expressed as:

$$Q = -\Delta H_{\text{vapor}} = -j_e \Delta h_{\text{lg}}, \tag{24}$$

where Δh_{lg} is the latent heat of evaporation. The evaporation water flux, j_e, can be calculated from:

$$j_e = \left(\frac{\xi}{0.84} \frac{p_{\text{sat}}(T)}{p_{\text{total}}} - 0.5 \right) \frac{I}{F}, \tag{25}$$

where the first term accounts roughly for the amount of water vapor present in the cathode exhaust and the second term describes the water vapor produced by ORR

at the cathode. Therefore, the net heat generation from a DMFC is given by:

$$Q_{\text{total}} = -\Delta h \cdot \frac{I + I_{x\,\text{over}}}{6F} - IV_{\text{cell}} - \left(\frac{\xi}{0.84}\frac{p_{\text{sat}}(T)}{p_{\text{total}}} - 0.5\right)\frac{I}{F}\Delta h_{\text{lg}}. \qquad (26)$$

This amount of heat must be removed either by circulating aqueous fuel solution (fuel cooling) or by air cooling from the stack peripherals. Much work remains to be done to analyze heat management in a DMFC and to understand how heat flow affects water management. It is expected that heat management will become a major technological challenge in development of portable DMFC power systems.

6 Mathematical modeling and experimental diagnostics

While attempts continue to elucidate the fundamental electrochemical reaction mechanisms, to explore new compositions and structures of catalysts, and to develop new membranes and methods to prevent methanol crossover, important system issues relevant to DMFC are emerging, such as water management, gas management, flow field design and optimization, and cell up-scaling for different applications. A number of physicochemical phenomena take place in liquid-feed DMFC, including species, charge, and momentum transfer, multiple electrochemical reactions, and gas-liquid two-phase flow in both anode and cathode. Carbon dioxide evolution in the liquid-feed anode results in strongly two-phase flow, making the processes of reactant supply and product removal more complicated. All these processes are intimately coupled, resulting in a need to search for optimal cell design and operating conditions. A good understanding of these complex, interacting phenomena is thus essential and can most likely be achieved through a combined mathematical modeling and detailed experimental approach. It is apparent that three of the four technical challenges for portable DMFC systems discussed in Section 1 require a basic understanding of methanol, water and heat transport processes occurring in DMFC. This provides a great opportunity to exercise fundamental modeling.

Another good topic for modeling is the micro DMFC system. Both anode carbon dioxide blockage and cathode flooding are especially acute in microsystems due to the small channel length scale involved, low operating temperature, dominance of surface tension forces, and requirement for low parasitic power losses in these systems [62–66]. More discussion on the general characteristics of micro DMFCs is presented in Section 7.

In addition, DMFC technology is a system requiring a high degree of optimization. A multitude of operating parameters affect the performance of a DMFC. These variables include cell temperature, molarity of aqueous methanol solution, cathode pressure, anode and cathode stoichiometry, and flow-field design. Higher cell temperatures improve catalytic activity, but increase water loss from the cathode. Efficient removal of carbon dioxide gas bubbles and liquid water produced on the anode and cathode, respectively, must be maintained to allow reactants to reach catalyst sites. Removal of carbon dioxide “slugs” and prevention of cathode

"flooding" can be attained by increasing flow rates. However, increasing flow rates requires more pumping power. Too high a flow rate on the cathode will dry out the polymer membrane, decreasing proton conductivity and hence cell performance. An understanding of the interdependence of these parameters plays a key role in optimizing the performance of a DMFC.

DMFC modeling thus aims to provide a useful tool for the basic understanding of transport and electrochemical phenomena in a DMFC and for the optimization of cell design and operating conditions. This modeling is challenging in that it entails the two-phase treatment for both anode and cathode, and in that both the exact role of the surface treatment in backing layers and the physical processes which control liquid phase transport are unknown.

6.1 Mathematical modeling

In the literature, Scott *et al.* [67–69] developed several simplified single-phase models to study transport and electrochemical processes in DMFC. Baxter *et al.* [70] developed a one-dimensional mathematical model for a liquid-feed DMFC anode. A major assumption of this study was that the carbon dioxide is only dissolved in the liquid and hence their anode model is a single-phase model. Using a macro-homogeneous model to describe the reaction and transport in the catalyst layer of a vapor-feed anode, Wang and Savinell [71] simulated the effects of the catalyst layer structure on cell performance. Kulikovsky *et al.* [72] simulated a vapor-feed DMFC with a two-dimensional model and compared the detailed current density distributions in the backing, catalyst layer, and membrane of a conventional to a novel current collector. In another paper, Kulikovsky [73] numerically studied a liquid-feed DMFC considering methanol transport through the liquid phase and in hydrophilic pores of the anode backing. In both publications of Kulikovsky, the important phenomenon of methanol crossover was ignored. Dohle *et al.* [74] presented a one-dimensional model for the vapor-feed DMFC and included the crossover phenomenon. The effects of methanol concentration on cell performance were studied.

In a three-part paper [75–77], Meyers and Newman developed a theoretical framework that describes the equilibrium of multicomponent species in the membrane. The transport of species in the membrane based on concentrated-solution theory and membrane swelling were taken into consideration in their model. The transport phenomena in the porous electrodes were also included in their mathematical model. However, the effect of pressure-driven flow was not considered. In addition, the transport of carbon dioxide out of the anode was neglected by assuming that the carbon dioxide was dilute enough to remain fully dissolved in liquid. Nordlund and Lindbergh [78] studied the influence of the porous structure on the anode with mathematic modeling and experimental verification. In their model, they also assumed that carbon dioxide does not evolve as gas within the electrode. Recently, Wang and Wang [79] presented a two-phase, multicomponent model. Capillary effects in both anode and cathode backings were accounted for. In addition to the anode and cathode electrochemical reactions, the model considered

diffusion and convection of both gas and liquid phases in backing layers and flow channels. The model fully accounted for the mixed potential effect of methanol oxidation at the cathode as a result of methanol crossover caused by diffusion, convection and electro-osmosis. The model of Wang and Wang was solved using a computational fluid dynamics technique and validated against experimental polarization curves. Results indicated the vital importance of gas phase transport in the DMFC anode. Divisek *et al.* [80] presented a similar two-phase, two-dimensional model of DMFC. Two-phase flow and capillary effects in backing layers were considered. In addition, detailed, multi-step reaction models for both ORR and MOR were developed. Murgia *et al.* [7] described a one-dimensional, two-phase, multi-component steady-state model based on phenomenological transport equations for the catalyst layer, diffusion layer, and polymer membrane for a liquid-feed DMFC.

Despite the fact that much effort has been made to model the DMFC system, considerable work remains, particularly in support of the emerging portable designs and systems. Few studies have treated the dominating effects of two-phase flow. No model to date has sufficient detail to provide a microfluidic theory for portable systems including effects of channel geometry and wettability characteristics of the GDL on fluid flow in the anode or cathode. Modeling studies are needed to fully elucidate the intricate couplings of methanol, water and heat transport processes. This understanding is key to successful design and operation of portable DMFC systems. Finally, although the important role of a micro-porous layer in DMFC and its tailoring to control the flow of methanol and water have begun to be recognized, much remains to be done.

6.2 Experimental diagnostics

Similarly, experimental diagnostics are an important component of DMFC development. Diagnostic techniques for DMFC have included:

- *cyclic voltammetry* (CV) to determine the electrochemically active area of the cathode,
- *CO stripping* to determine the electrochemically active area of the anode,
- *electrochemical impedance spectroscopy* (EIS),
- *anode polarization* characterization via a CH_3OH/H_2 cell as proposed by Ren *et al.* [28],
- *methanol crossover* rate measurement by CO_2 sensing in the cathode (via FITR, GC or infrared CO_2 sensors), or by measuring the limiting current in a CH_3OH/N_2 cell (Ren *et al.* [28]),
- *current distribution* measurements via a segmented cell in conjunction with a multi-channel potentiostat (Mench and Wang [40]), and
- *material balance analysis* of CH_3OH and H_2O (Narayanan *et al.* [17] and Muller *et al.* [18]).

In addition, two-phase visualization of bubble dynamics [5, 31, 32] on anode and liquid droplet dynamics on cathode [32] as described in Sections 3.1.1 and 3.2.2, respectively, is a useful tool for cell design and optimization.

Mench and Wang [40] described an experimental technique to measure current distribution in a 50 cm^2 instrumented DMFC based on a segmented cell and multi-channel potentiostat. In this method, separate current collector ribs are embedded into an insulating substrate (e.g. Lexan plate) to form a segmented flowfield plate. The resulting flowfield plates for both anode and cathode are then assembled with a regular MEA to form a fuel cell with independently controllable subcells. All subcells are connected to a multi-channel potentiostat to undergo potentiostatic experiments simultaneously. The subcell currents measured thus provide information on the current density distribution for the full-scale fuel cell. The spatial and temporal resolution of this method depends on the number of channels available and capabilities of the potentiostat. Current density distribution measurements were made for a wide range of cathode flow rates in order to elucidate the nature of cathode flooding in the DMFC. Figure 17 displays the current density distributions for a high and a low cathode air flow rates, respectively. In the case of high cathode stoichiometry (Fig. 17(a)), it can be seen that the current is rather uniform for all three cell voltages. As expected, the current density increases as the cell voltage decreases. In the case of low cathode stoichiometry (still excessive for the oxygen reduction reaction), Fig. 17(b) clearly shows that a portion of the cathode towards the exit is fully flooded, leading to almost zero current. The information provided in Fig. 17 can be used to identify innovative cathode flowfield designs and enables the development of MEA structures with improved water management capabilities.

Material balance analysis proves to be a critical diagnostic tool for the development of portable DMFC systems. In this analysis, methanol balance on the anode side along with the methanol crossover rate typically measured by an infrared CO_2 sensor is conducted. In addition, water balance on both anode and cathode sides is performed, where cathode water is carefully collected by a moisture trap and measured [17, 18, 59]. From such analyses, Müller *et al.* [18] revealed that the

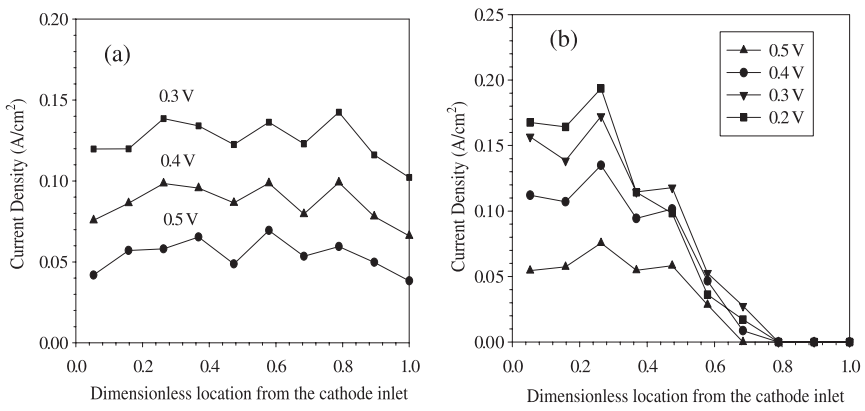

Figure 17: Current density distributions in a 50 cm^2 DMFC for: (a) high cathode air flowrate (stoichiometry of 85 @ 0.1 A/cm^2) and (b) low cathode air flowrate (stoichiometry of 5 @ 0.1 A/cm^2).

water balance on the DMFC anode is highly negative, thus calling for membrane development with low water crossover in addition to low methanol crossover.

6.3 Model validation

Experimental validation of the two-phase DMFC model of Wang and Wang [79] has been carried out for a 5 cm^2 graphite cell. A brief description of the cell geometry, MEA compositions and operating conditions is given in Fig. 18. Figure 18(a) illustrates the capability of the model to predict the polarization curves at two cell temperatures. Excellent agreement is achieved not only in the kinetic- and ohmic-controlled regions of the polarization curves but also in the mass transport controlled region, where the methanol oxidation kinetics is modeled as a zero-order reaction for molar concentrations above 0.1 M, but a first-order reaction for a molarity below 0.1 M. This shift in the reaction order and the molarity of transition is consistent with direct kinetics measurements. A lower mass transport limiting current density at 50 °C, seen from Fig. 18(a), is caused by the lower diffusion coefficients in both liquid and gas phases and the lower saturation methanol vapor concentration in the gas phase at lower temperatures. Using the same model and physical property data, Fig. 18(b) shows equally satisfactory agreement in the polarization curves between numerical and experimental results for different methanol feed concentrations. In accordance with these experiments, the model prediction for the 2 M case shows a slightly lower performance (due primarily to higher methanol crossover) and an extended limiting current density. Similar success in validating global *I-V* curves was also reported by Murgia *et al.* [7], among others.

While the model validation against cell overall performance data has been satisfactory and encouraging, as evident from Fig. 18, the ultimate test of these highly sophisticated two-phase models is comparison with detailed distribution

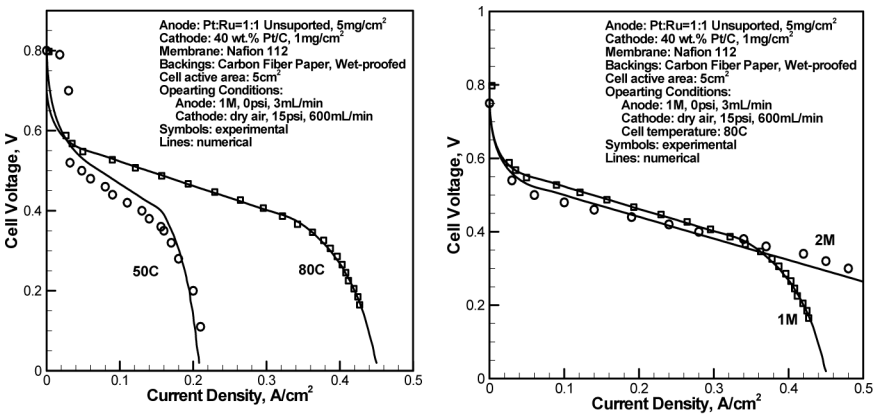

(a) Temperature Effect (b) Concentration Effect

Figure 18: Comparisons of 2-D model predictions with experimental data for a DMFC with: (a) temperature effect and (b) concentration effect.

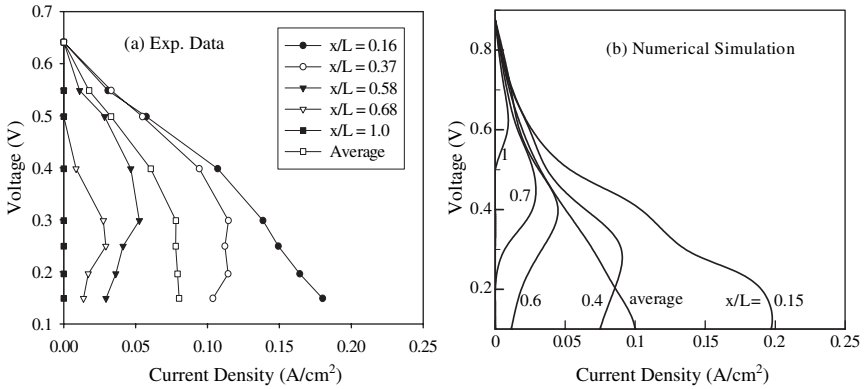

Figure 19: Comparison of localized polarization curves between experiments (a) and model predictions (b) for a 50 cm^2 DMFC with the anode flow stoichiometry of 27 and cathode air stoichiometry of 5 @ 0.1 A/cm^2.

measurements. Figure 19 presents such an attempt toward developing high-fidelity, first-principles models for DMFC. Figure 19(a) shows a set of localized polarization curves measured using the current distribution measurement technique of Mench and Wang [40], and Fig. 19(b) displays the same set of polarization curves predicted from the DMFC two-phase model of Wang and Wang [79]. A low air stochiometry of 5 (although not low for the electrochemical reaction requirement) was deliberately chosen so that cathode GDL flooding may occur and a non-uniform current density distribution results.

The two graphs in Fig. 19 share a qualitative similarity. For example, both experiment and model results indicate that the local polarization curves near the dry air inlet exhibit a monotonic function between the voltage and current. Also, the shape of the polarization curves near the exit, from both experiment and simulation, is clearly evidence of flooding in the cathode GDL. Another interesting observation is that the average cell polarization curves, measured and predicted, do not exhibit any sign of cathode flooding, indicating that detailed distribution measurements are absolutely required in order to discern complex physicochemical phenomena occurring inside the cell. Finally, it can be seen from Fig. 19 that a satisfactory quantitative comparison between experiment and model is lacking on the detailed level.

Difficulties in obtaining good quantitative agreement between predicted and measured distribution results are indicative that model refinements as well as an improved property data base will be needed before accurate quantitative predictions of not only overall polarization curve but also detailed distributions within a DMFC may be obtained.

7 Application: micro DMFC

Micro-power sources are a key technology in future integrated micro-systems that enable sensing, computing, actuation, control, and communication on a single chip.

Due to such advantages as easy storage of liquid fuel, ambient temperature operation, and simple construction, the direct methanol fuel cell has received much attention as a leading candidate for micro-power sources of the future [17].

Thanks to the integrated-circuit (IC) fabrication technology, micro-channel patterns of DMFC bipolar plates into which reactants are fed can be featured on the silicon wafer with high resolution and good repeatability. Kelley *et al.* [81] reported a 0.25 cm^2 micro DMFC using silicon (Si) wafer as the substrate. The anode catalyst in their micro DMFC was prepared by coelectrodepositing a Pt-Ru alloy onto a carbon coated Si wafer. Using 0.5 M methanol solution, the micro DMFC was tested and yielded an output current density very close to that of large-scale DMFC. In a subsequent paper [62], they reported that a prototype cell (12 mm^3 in volume) micro-fabricated on Si substrates and featuring electrodeposition of Pt-Ru as the anode catalyst successfully demonstrated a lowering of catalyst loading to 0.25 mg/cm^2 without loss of performance. Pavio *et al.* instead explored low-temperature co-fired ceramic (LTCC) material as an alternative for the bipolar plates of micro fuel cell system, and a DMFC prototype, packaged using LTCC, was reported in their paper [64].

In addition, micro PEM fuel cells based on a Si wafer using microelectromechanical system (MEMS) technology have been under extensive development [66, 82–85]. Lee *et al.* [66] reported a micro fuel cell design in which a planar array of cells are connected in series in a "flip-flop" configuration. Maynard and Meyers [82] proposed a conceptual design for a miniaturized DMFC for powering 0.5–20 W portable telecommunication and computing devices. Heinzel *et al.* [83] demonstrated a prototype miniature fuel cell stack to power a laptop computer using hydrogen and air as reactants running at ambient pressure and temperature. Most recently, Yu *et al.* [84, 85] fabricated a miniature twin-fuel-cell connected in series by sandwiching two membrane-electrode-assemblies between two Si micromachined plates.

In the recent work of Lu *et al.* [10], the fabrication process of the silicon wafer is illustrated in Fig. 20. Figure 21 shows a picture of the silicon wafer with fabricated flow channel pattern. The fluid channels in the Si wafer have a depth of 400 μm. Both the flow channel and the rib separating two neighboring channels were 750 μm wide, with the channel length of 12.75 mm. There were a total of nine channels with serpentine flowfield, forming a cell effective area of approximately 1.625 cm^2. In order to collect current and to minimize contact resistance between the MEA and the Si wafer, Ti/Cu/Au (with thickness of 0.01/3/0.5 μm) was deposited on the front-side of each wafer by electron beam evaporation.

Figure 22 shows a series of cell polarization curves operated at different temperatures using 1 M methanol solution under ambient pressure in the Si-based micro DMFC [10]. The flow rate of non-preheated air was 88 mL/min and the methanol feed rate was 2.83 mL/min. The maximum power density of the cell reached 14.27 mW/cm^2 at a voltage of 0.196 V at room temperature (i.e. 23 °C). The maximum power density was 24.75 mW/cm^2 at a voltage of 0.214 V when the temperature increased to 40 °C. This is because the kinetics of electrodes, particularly methanol oxidation at the anode, is enhanced at elevated temperatures. For the

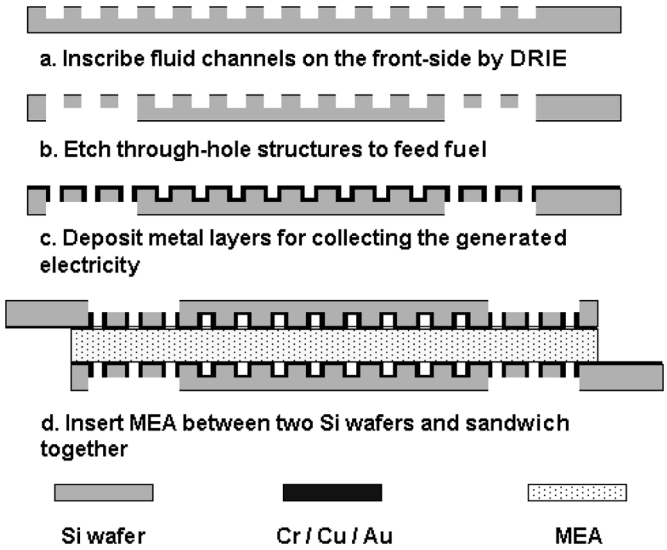

Figure 20: Fabrication process flow of the μDMFC.

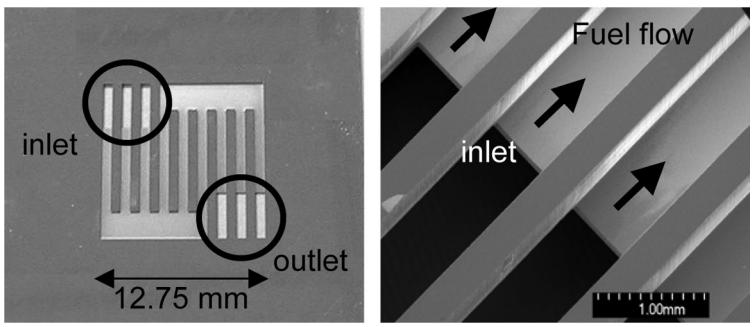

Figure 21: A silicon wafer with flow channels.

same reason, maximum power density was 47.18 mW/cm^2 at a voltage of 0.258 V and temperature of 60 °C.

A problem emerging in Si-based micro DMFCs is that the silicon substrate is too fragile and it becomes difficult to compress the cell tightly for sealing and to reduce the contact resistance between the MEA and flow plates. In addition, a thick gold layer has to be coated on Si substrate to improve the conductivity as a current collector. Alternatively, one can use photochemical etching of stainless steel to fabricate the flow plate/current corrector instead of silicon wafer [86]. Stainless steel provides much higher conductivity than silicon, thus avoiding thicker metal coating on the surface. Also, photochemical etching is a simple, high-quality, fast-turnaround, low-cost process for micro-fabrication of flow channels on stainless steel.

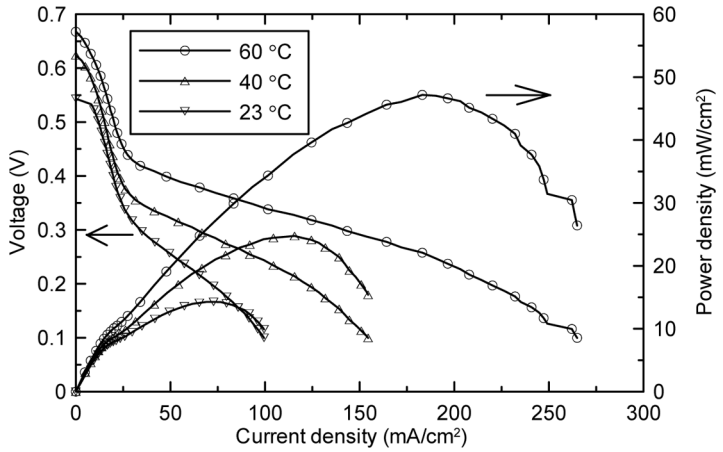

Figure 22: Polarization and power density curves at different temperatures using 1 M methanol solution with the air flow rate of 88 mL/min and methanol flow rate of 2.83 mL/min at atmospheric pressure.

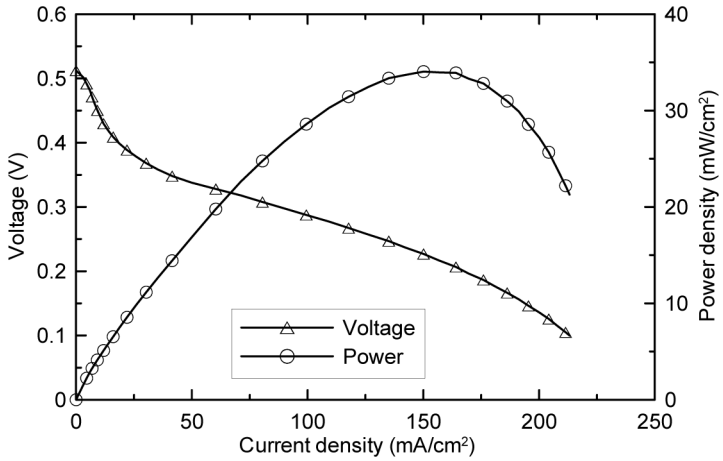

Figure 23: Polarization curve using 2 M methanol solution at 22 °C, air flow rate of 161 mL/min, methanol flow rate of 2.2 mL/min, and ambient pressure.

Figure 23 shows the polarization and power density curves using 2 M methanol solution at 22 °C and atmospheric pressure. The flow plates in this DMFC were made of stainless steel using the photochemical etching method. The flowfield and cell size were identical to the Si-based micro DMFC reported before [10]. The methanol flow rate was 2.2 mL/min, and the air flow rate was 161 mL/min. At room temperature, the current density reach 90 mA/cm^2 at 0.3 V and the maximum power density was 34 mW/cm^2 at 0.23 V. Figure 24 displays the polarization and power density curves of the same stainless steel cell using 2 M methanol solution

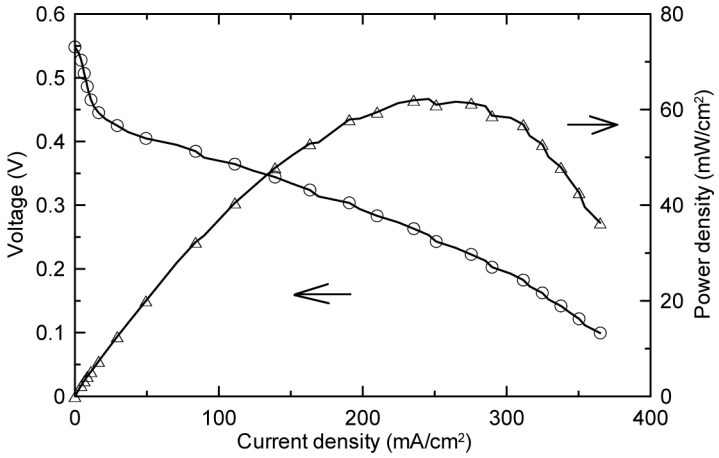

Figure 24: Polarization curve using 2 M methanol solution at 40 °C, air flow rate 161 mL/min, methanol flow rate 2.2 mL/min, and ambient pressure.

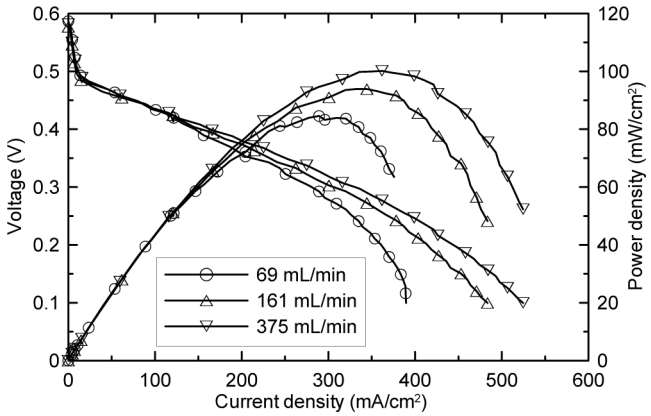

Figure 25: Polarization curve using 2 M methanol solution at 60 °C at different air flow rates, methanol flow rate 2.2 mL/min, and ambient pressure.

at 40 °C and atmospheric pressure. The cell performance reach about 200 mA/cm^2 at 0.3 V and the maximum power density was 62.5 mW/cm^2 at 0.26 V.

Figure 25 shows the polarization and power density curves using different air flow rates. The methanol flow rate was fixed at 2.2 mL/min. At low current densities, the cell voltages are almost identical under different air flow rates. The overall cell performance improves with the air flow rate increasing. At the air flow rate of 375 mL/min, the cell performance reach 330 mA/cm^2 at 0.3 V and the maximum power density was 100 mW/cm^2 at 0.28 V.

Figure 26 displays the anode polarization behaviors at different temperatures when hydrogen was used in the cathode. As expected, the anode overpotential

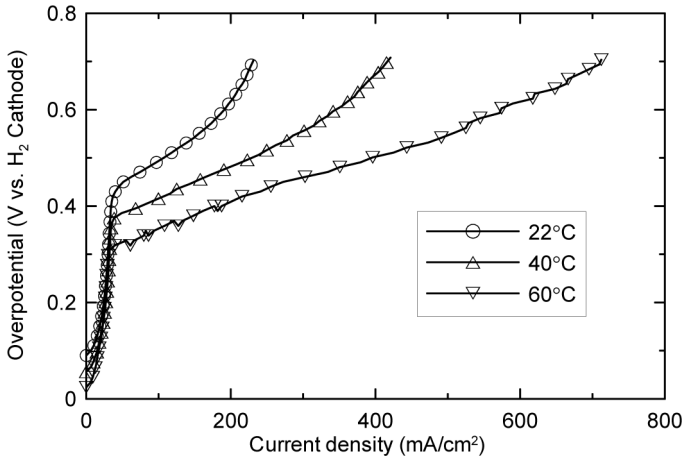

Figure 26: Anode overpotential with hydrogen cathode, 2 M methanol with flow rate of 2.2 mL/min, hydrogen flow rate 161 mL/min, and ambient pressure.

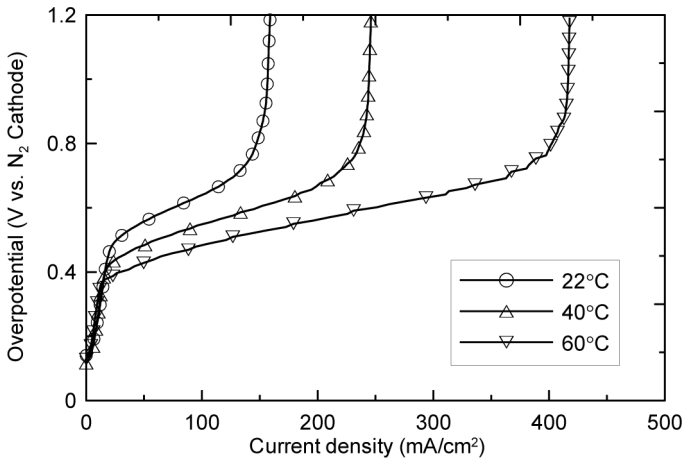

Figure 27: Methanol crossover rate at open circuit voltage, 2 M Methanol with flow rate of 2.2 mL/min, nitrogen flow rate 161 mL/min, and ambient pressure.

decreased as the temperature increased. Using this H_2-evolving counter electrode, the anode overpotential may deviate somewhat from the real kinetic results using dynamic hydrogen electrode [28]. However, using the H_2-evolving cathode is still a simple and useful method to evaluate and screen the anode characteristics in an assembled DMFC.

Figure 27 shows the polarization behavior when air was replaced by humidified nitrogen in the cathode. Such cells, consisting of MeOH anode and N_2 cathode,

allow measurement of the methanol crossover rate. As methanol diffuses from the anode side to the cathode side, the electrochemical reaction at the N_2 cathode becomes:

$$CH_3OH + H_2O \rightarrow CO_2 + 6H^+ + 6e^-.$$

Protons produced from the above reaction then migrate back to the anode side of the membrane where they are combined to evolve H_2. That is:

$$6H^+ + 6e^- \rightarrow 3H_2.$$

Thus, the methanol crossover rate at the open circuit voltage can be determined from the limiting current density observed from the polarization behavior of such a cell [28]. It is seen from Fig. 27 that the methanol crossover rate is relatively large with the small MEA area due to edge leakage [86].

To summarize, micro DMFCs fabricated by photochemical etching of stainless steel have attained impressive performance (i.e. 100 mW/cm^2 at 60 °C) for high-power applications. For future development, it is necessary to further lower the air and fuel feeding rates so as to reduce the pumping power. In this regard, a self-activated micro DMFC holds much promise where the cathode is air breathing and the anode features a pumpless delivery of liquid fuel. Further development in micro-DMFCs is to decrease the system volume and increase the methanol concentration in the fuel tank and hence the energy density.

8 Summary and outlook

The fundamental transport processes of methanol, water and heat occurring in DMFCs for micro and portable applications have been reviewed, along with a summary of recent DMFC models and diagnostic techniques. Significant challenges still exist before a DMFC can compete with the latest Li-ion battery technology. We have stressed in this chapter that a better understanding of the basic transport phenomena achieved through combined flow visualization studies and transport simulations is essential to overcome these challenges and to inspire new design concepts. We demonstrated that, contrary to conventional wisdom, a DMFC based on thin Nafion 112 membrane can reach a fuel efficiency of ~80% and a water crossover coefficient lower than unity while still maintaining a power density of 56 mW/cm^2 at 60 °C and ambient air.

Two-phase modeling capabilities for DMFC have emerged, which unravel the importance of gas phase transport of methanol as compared to the liquid phase transport. In addition, much effort is being directed towards developing a coupled model for methanol, water and heat transport processes simultaneously in a DMFC. Such models are extremely useful for the discovery of unique design and operation regimes of the DMFC system for portable application, where the high energy density entails using highly concentrated methanol (preferably pure methanol), maintaining low water and methanol crossover, and improving high-voltage performance. The latter two factors will result in high efficiency DMFCs. It is expected that the DMFC model development will be directed less towards refining model accuracy

or improving computational speed, but more towards applying the models to invent new cell designs and pinpoint areas of improvement.

Other important research issues such as an accurate materials data base were discussed in Wang [87].

References

[1] Boslet, S.W., *Experimental study of a direct methanol fuel cell*, M.S. thesis, The Pennsylvania State University, 2001.

[2] Halpert, G., Narayanan, S.R., Valdez, T., Chun, W., Frank, H., Kindler, A., Surampudi, S., Kosek, J., Cropley C. & LaConti, A., Progress with the direct methanol liquid-feed fuel cell system. *Proc. of the 32nd Intersociety Energy Conversion Engineering Conference*, 2, AIChE: New York, pp. 774–778, 1997.

[3] Baldauf, M. & Preidel, W., Status of the development of a direct methanol fuel cell. *Journal of Power Sources*, **84**, pp. 161–166, 1999.

[4] Ren, X., Zelenay, P., Thomas, S., Davey, J. & Gottesfeld, S., Recent advances in direct methanol fuel cells at Los Alamos National Laboratory. *Journal of Power Sources*, **86**, pp. 111–116, 2000.

[5] Scott, K., Taama, W.M. & Argyropoulos, P., Carbon dioxide evolution patterns in direct methanol fuel cells. *Electrochimica Acta*, **44**, pp. 3575–3584, 1999.

[6] Scott, K., Mass transfer in flow fields. *Handbook of Fuel Cells*, eds W. Vielstich, H.A. Gasteiger & A. Lamm, John Wiley and Sons Ltd.: England, **1**, p. 70, 2003.

[7] Murgia, G., Pisani, L., Shukla, A.K. & Scott, K., A numerical model of a liquid-feed Solid polymer electrolyte DMFC and its experimental validation. *Journal of the Electrochemical Society*, **150**, pp. A1231–A1245, 2003.

[8] Mench, M., Boslet, S., Thynell, S., Scott, J. & Wang, C.Y., Experimental study of a direct methanol fuel cell. *Direct Methanol Fuel Cells*, The Electrochemical Society Proceedings Series: Pennington, NJ, 2001.

[9] Lim, C. & Wang, C.Y., Development of high power electrodes for a liquid-feed direct methanol fuel cell. *Journal of Power Sources*, **113**, pp. 145–150, 2003.

[10] Lu, G.Q., Wang, C.Y., Yen, T.J. & Zhang, X., Development and characterization of a silicon-based micro direct methanol fuel cell. *Electrochimica Acta*, **49**, pp. 821–828, 2004.

[11] Yen, T.J., Fang, N., Zhang, X., Lu, G.Q. & Wang, C.Y., A micro direct methanol fuel cell operating at near room temperature. *Applied Physics Letters*, **83**, pp. 4056–4058, 2003.

[12] Gottesfeld, S. & Wilson, M.S., Polymer electrolyte fuel cells as potential power sources for portable electronic devices. *Energy Storage Systems for Electronics Devices*, eds T. Osaka & M. Datta, Gordon and Breach Science Publishers: Singapore, p. 487, 2000.

[13] Gottesfeld, S. & Zawodzinski, T.A., *Adv. in Electrochemical Science and Engineering*, ed. C. Tobias, Vol. 5, Wiley and Sons: New York, 1997.
[14] Lamy, C., Leger, J.-M. & Srinivasan, S., *Modern Aspects of Electrochemistry*, eds J. Bockris & O'M *et al.*, Kluwer Academic/Plenum Publishers: New York, p. 53, 2001.
[15] Arico, A.S., Srinivasan, S. & Antonucci, V., DMFCs: From fundamental aspects to technology development. *Fuel Cells*, **1**, pp. 133–161, 2001.
[16] Neergat, M., Friedrich, K.A. & Stimming, U., New material for DMFC MEAs. *Handbook of Fuel Cells*, eds W. Vielstich, H.A. Gasteiger & A. Lamm, John Wiley and Sons Ltd.: England, Chap 63, pp. 856–877, 2003.
[17] Narayanan, S.R., Valdez, T.I. & Rohatgi, N., DMFC system design for portable applications. *Handbook of Fuel Cells*, eds W. Vielstich, H.A. Gasteiger & A. Lamm, John Wiley and Sons Ltd.: England, Chapter 65, pp. 894–904, 2003.
[18] Müller, J., Frank, G., Colbow, K. & Wilkinson, D., Transport/kinetic limitations and efficiency losses. *Handbook of Fuel Cells*, eds W. Vielstich, H.A. Gasteiger & A. Lamm, John Wiley and Sons Ltd.: England, Chap 62, pp. 847–855, 2003
[19] Pasaogullari, U. & Wang, C.Y., Two-phase transport and the role of microporous layer in polymer electrolyte fuel cells. *Electrochimica Acta*, submitted for publication: 2004.
[20] Barendrecht, E., Electrochemistry of fuel cells. *Fuel cell systems*, eds L.J.M.J. Blomen & M.N. Mugerwa, New York, p. 75, 1993.
[21] Wasmus, S. & Kuver, A., Methanol oxidation and direct methanol fuel cells: a selective review. *Journal of Electrochemical Society*, **461**, pp. 14–31, 1999.
[22] Lin, W.F., Wang, J.T. & Savinell, R.F., On-line FTIR Spectroscopic investigations of methanol oxidation in a direct methanol fuel cell. *Journal of the Electrochemical Society*, **144**, pp. 1917–1922, 1997.
[23] Hamnett, A., Mechanism and electrocatalysis in the direct methanol fuel cell. *Catalysis Today*, **38**, pp. 445–457, 1997.
[24] Thomas, S.C., Ren, X. & Gottesfeld, S., Influence of ionomer content in catalyst layers on direct methanol fuel cell performance. *Journal of the Electrochemical Society*, **146**, pp. 4354–4359, 1999.
[25] Liu, L., Pu, C., Viswanathan, R., Fan, Q., Liu, R. & Smotkin, E.S., Carbon supported and unsupported Pt-Ru anodes for liquid feed direct methanol fuel cells. *Electrochimica Acta*, **43**, pp. 3657–3663, 1998.
[26] Hayden, E., The promotion of CO electro-oxidation on platinum-bismuth as a model for surface mediated oxygen transfer. *Catalysis Today*, **38**, pp. 473–481, 1997.
[27] Page, T., Johnson, R., Hormes, J., Noding, S. & Rambabu, B., A study of methanol electro-oxidation reactions in carbon membrane electrodes and structural properties of Pt alloy electro-catalysts by EXAFS. *Journal of Electroanalytical Chemistry*, **485**, pp. 34–41, 2000.

[28] Ren, X., Springer, T.E. & Gottesfeld, S., Water and methanol uptakes in nafion membranes and membrane effects on direct methanol cell performance. *Journal of the Electrochemical Society*, **147**, pp. 92–98, 2000.
[29] Arico, S., Creti, P., Modica, E., Monforte, G., Baglio, V. & Antonucci, V., Investigation of direct methanol fuel cells based on unsupported Pt–Ru anode catalysts with different chemical properties. *Electrochimica Acta*, **45**, pp. 4319–4328, 2000.
[30] Ravikumar, M.K. & Shukla, A.K., Effect of methanol crossover in a liquid-feed Polymer-electrolyte direct methanol fuel cell. *Journal of the Electrochemical Society*, **143**, pp. 2601–2605, 1996.
[31] Apgyropoulos, R., Scott, K. & Taama, W.M., Gas evolution and power performance in direct methanol fuel cells. *Journal of Applied Electrochemistry*, **29**, pp. 663–671, 1999.
[32] Lu, G.Q. & Wang, C.Y., Electrochemical and flow characterization of a direct methanol fuel cell. *Journal of Power Sources*, **134**, pp. 33–40, 2004.
[33] Wallis, G.B., *One Dimensional Two-Phase Flow*, McGraw-Hill: New York, 1969.
[34] Mathias, M.F., Roth, J., Fleming, J. & Lehnert, W., Diffusion media material and characterisation. *Handbook of Fuel Cells – Fundamental, Technology and Application*, eds W. Vielstich, A. Lamm & H.A. Gasteiger, Volume 3, John Wiley & Sons, pp. 517–537, 2003.
[35] Whalley, P.B., *Boiling, Condensation and Gas-Liquid Flow*, Clarendon press: Oxford, p. 16, 1987.
[36] Springer, T.E., Zawodzinski, T.A. & Gottesfeld, S., Polymer electrolyte fuel cell model. *Journal of the Electrochemical Society*, **138**, pp. 2334–2341, 1991.
[37] Wang, Z.H., Wang, C.Y. & Chen, K.S., Two-phase flow and transport in the air cathode of proton exchange membrane fuel cells. *Journal of Power Sources*, **94**, pp. 40–50, 2001.
[38] Wang, C.Y., Two-phase flow and transport. *Handbook of Fuel Cells*, eds W. Vielstich, H.A. Gasteiger & A. Lamm, John Wiley and Sons Ltd.: England, **3**, pp. 337–348, 2003.
[39] Yang, X.G., Zhang, F.Y., Lubawy, A. & Wang, C.Y., Visualization of liquid water transport in a polymer electrolyte fuel cell. *Electrochemical & Solid-State Letters*, in press, 2004.
[40] Mench, M.M. & Wang, C.Y., An *in situ* method for determination of current distribution in PEM fuel cells applied to a direct methanol fuel cell. *Journal of the Electrochemical Society*, **150**, pp. A79–A85, 2003.
[41] Ren, X. & Gottesfeld, S., Electro-osmotic drag of water in poly(perfluorosulfonic acid) membranes. *Journal of the Electrochemical Society*, **148**, pp. A87–A93, 2001.
[42] Narayanan, S.R., Frank, H., Jeffries-Nakamura, B., Smart, M., Chun, W., Halpert, G., Kosek, J. & Cropley, C., *Proton Conducting Membrane Fuel Cells I*, eds S. Gottesfeld, G. Halpert & A. Landgrebe, The Electrochemical Society Proceedings Series: Pennington, NJ, PV 95-23, p. 278, 1995.

[43] Ren, X., Zawodzinski, T.A., Uribe, F., Dai, H. & Gottesfeld, S., *Proton Conducting Membrane Fuel Cells I*, eds S. Gottesfeld, G. Halpert & A. Landgrebe, The Electrochemical Society Proceedings Series: Pennington, NJ, PV 95-23, p. 284, 1995.

[44] Ren, X., Springer, T.E., Zawodzinski, T.A. & Gottesfeld, S., Methanol transport through nation membranes, electro-osmotic drag effects on potential step measurements. *Journal of the Electrochemical Society*, **147**, pp. 466–474, 2000.

[45] Valdez, T.I. & Narayanan, S.R., *Proton Conducting Membrane Fuel Cells II*, eds S. Gottesfeld, T.F. Fuller & G. Halpert, The Electrochemical Society Proceedings Series: Pennington, NJ, PV 98-27, p. 380, 1998.

[46] Wang, J.T., Wasmus, S. & Savinell, R.F., Real-Time Mass spectrometric study of the methanol crossover in a direct methanol fuel cell. *Journal of the Electrochemical Society*, **143**, pp. 1233–1239, 1996.

[47] Kauranen, P.S. & Skou, E., Mixed methanol oxidation/oxygen reduction currents on a carbon supported Pt catalyst. *Journal of Electroanalytical Chemistry*, **408**, pp. 189–198, 1996.

[48] Kuver, A. & Vielstich, W., Investigation of methanol crossover and single electrode performance during PEMDMFC operation – A study using a solid polymer electrolyte membrane fuel cell system. *Journal of Power Sources*, **74 (2)**, pp. 211–218, 1998.

[49] Scott, K., Taama, W.M., Argyropoulos, P. & Sundmacher, K., The impact of mass transport and methanol crossover on the direct methanol fuel cell. *Journal of Power Sources*, **83(1–2)**, pp. 204–216, 1999.

[50] Garau, B. & Smotkin, E.S., Methanol crossover in direct methanol fuel cells: a link between power and energy density. *Journal of Power Sources*, **112**, pp. 339–352, 2002.

[51] Heinzel, A. & Barragan, V.M., A review of the state-of-the-art of the methanol crossover in direct methanol fuel cells. *Journal of Power sources*, **84**, pp. 70–74, 1999.

[52] Peled, E., Duvdevani, T., Aharon, A. & Melman, A., A direct methanol fuel cell based on a novel low-cost nanoporous proton-conducting membrane. *Electrochemical and Solid State Letters*, **3(12)**, pp. 525–528, 2000.

[53] Nunes, S.P., Ruffmann, B., Rikowski, E., Vetter, S. & Richau, K., Inorganic modification of proton conductive polymer membranes for direct methanol fuel cells. *Journal of Membrane Science*, **203(1–2)**, pp. 215–225, 2002.

[54] Yamaguchi, T., Ibe, M., Nair, B.N. & Nakao, S., A pore-filling electrolyte membrane-electrode integrated system for a direct methanol fuel cell application. *Journal of the Electrochemical Society*, **149(11)**, pp. A1448–A1453, 2002.

[55] Pan, Y., Ph.D. Thesis, The Pennsylvania State University, 2004.

[56] Peled, E., Blum, A., Aharon, A., Philosoph, M. & Lavi, Y., Novel approach to recycling water and reducing water loss in DMFCs. *Electrochemical and Solid-State Letters*, **6**, pp. A268–A271, 2003.

[57] Blum, A., Duvdevani, T., Philosoph, M., Rudoy, N. & Peled, E., Water-neutral micro direct-methanol fuel cell (DMFC) for portable applications. *Journal of Power Sources*, **117**, pp. 22–25, 2003.

[58] Pasaogullari, U. & Wang, C.Y., Liquid water transport in gas diffusion layer of polymer electrolyte fuel cells. *Journal of the Electrochemical Society*, **151**, pp. A399–A406, 2004.

[59] Lu, G.Q., Liu, F.Q. & Wang, C.Y., Water transport through Nafion 112 membrane in direct methanol fuel cells. *Electrochemical & Solid-State Letters*, **8(1)**, pp. A1–A4, 2005

[60] Argyropoulos, P., Scott, K. & Taama, W.M., One-dimensional thermal model for direct methanol fuel cell stacks Part I. Model development. *Journal of Power Sources*, **79**, pp. 169–183, 1999.

[61] Dohle, H., Mergel, J. & Stolten, D., Heat and power management of a direct-methanol-fuel-cell (DMFC) system. *Journal of Power Sources*, **111**, pp. 268–282, 2002.

[62] Kelley, S.C., Deluga, G.A. & Smyrl, W.H., Miniature fuel cells fabricated on silicon substrates. *AICHE J*, **48**, pp. 1071–1082, 2002.

[63] Mench, M.M., Wang, Z.H., Bhatia, K. & Wang, C.Y., Design of a micro direct methanol fuel cell. *Proceedings of the International Mechanical Engineering Congress and Exposition (IMECE)*, November 11–16, 2001.

[64] Pavio, J., Bostaph, J., Fisher, A., Hallmark, J., Mylan, B.J. & Xie, C.G., LTCC fuel cell system for portable wireless electronics. *Advancing Microelectronics*, **29**, pp. 1–8, 2002.

[65] Dyer, C.K., Fuel cells for portable applications. *Journal of Power Sources*, **106**, pp. 31–34, 2002.

[66] Lee, S.J., Chang-Chien, A., Cha, S.W., O'Hayre, R., Park, Y.I., Saito, Y. & Prinz, F.B., Design and fabrication of a micro fuel cell array with 'flip-flop' interconnection. *Journal of Power Sources*, **112**, pp. 410–418, 2002.

[67] Scott, K., Argyropoulos, P. & Sundmacher, K., A model for the liquid feed direct methanol fuel cell. *Journal of Electroanalytical Chemistry*, **477**, pp. 97–110, 1999.

[68] Sundmacher, K. & Scott, K., Direct methanol polymer electrolyte fuel cell: Analysis of charge and mass transfer in the vapour–liquid–solid system. *Chemical Engineering Science*, **54**, pp. 2927–2936, 1999.

[69] Argyropoulos, P., Scott, K. & Taama, W. M., Hydrodynamic modelling of direct methanol liquid feed fuel cell stacks. *Journal of Applied Electrochemistry*, **30**, pp. 899–913, 2000.

[70] Baxter, S.F., Battaglia, V.S. & White, R.E., Methanol fuel cell model: anode. *Journal of the Electrochemical Society*, **146**, pp. 437–447, 2000.

[71] Wang, J. & Savinell, R.F., *Electrode Materials and Processes for Energy Conversion and Storage*, eds S. Srinivasan, D.D. Macdonald & A.C. Khandkar, The Electrochemical Society Proceedings Series: Pennington, NJ, PV 94–23, p. 326, 1994.

[72] Kulikovsky, A.A., Divisek, J. & Kornyshev, A.A., Two-dimensional simulation of direct methanol fuel cell a new (embedded) type of current collector. *Journal of the Electrochemical Society*, **147**, pp. 953–959, 2000.
[73] Kulikovsky, A.A., Two-dimensional numerical modelling of a direct methanol fuel cell. *Journal of Applied Electrochemistry*, **30(9)**, pp. 1005–1014, 2000.
[74] Dohle, H., Divisek, J. & Jung, R., Process engineering of the direct methanol fuel cell. *Journal of Power Sources*, **86**, pp. 469–477, 2000.
[75] Meyers, J.P. & Newman, J., Simulation of the direct methanol fuel cell I. Thermodynamic framework for a multicomponent membrane. *Journal of the Electrochemical Society*, **149**, pp. A710–A717, 2002.
[76] Meyers, J.P. & Newman, J., Simulation of the direct methanol fuel cell II. Modeling and data analysis of transport and kinetic phenomena. *Journal of the Electrochemical Society*, **149**, pp. A718–A728, 2002.
[77] Meyers, J.P. & Newman, J., Simulation of the direct methanol fuel cell III. Design and optimization. *Journal of the Electrochemical Society*, **149**, pp. A729–A735, 2002.
[78] Nordlund, J. & Lindbergh, G., A model for the porous direct methanol fuel cells anode. *Journal of the Electrochemical Society*, **149**, pp. A1107–A1113, 2002.
[79] Wang, Z.H. & Wang, C.Y., Mathematical modeling of liquid-feed direct methanol fuel cells. *Journal of the Electrochemical Society*, **150**, pp. A508–A519, 2003.
[80] Divisek, J., Fuhrmann, J., Gartner, K. & Jung, R., Performance modeling of a direct methanol fuel cell. *Journal of the Electrochemical Society*, **150**, pp. A811–A825, 2003.
[81] Kelley, S.C., Deluga, G.A. & Smyrl, W.H., A miniature methanol/air polymer electrolyte fuel cell. *Electrochemical and Solid-State Letters*, **3**, pp. 407–409, 2000.
[82] Maynard, H.L. & Meyers, J.P., Miniature fuel cells for portable power: design considerations and challenges. *The Journal of Vacuum Science and Technology B*, **20**, pp. 1287–1297, 2002.
[83] Heinzel, A., Hebling, C., Muller, C., Zedda, M.M. & Muller, C., Fuel cells for low power applications. *Journal of Power Sources*, **105**, pp. 250–255, 2002.
[84] Yu, J.R., Cheng, P., Ma, Z.Q. & Yi, B.L., Fabrication of a miniature twin-fuel-cell on silicon wafer. *Electrochimica Acta*, **48**, pp. 1537–1541, 2003.
[85] Yu, J.R., Cheng, P., Ma, Z.Q. & Yi, B.L., Fabrication of miniature silicon wafer fuel cells with improved performance. *Journal of Power Sources*, **124(1)**, pp. 40–46, 2003.
[86] Lu, G.Q. & Wang, C.Y., Development of micro direct methanol fuel cells for high power applications. *Journal of Power Sources*, in press.
[87] Wang, C.Y., Fundamental models for fuel cell engineering. *Chemical Reviews*, **104**, pp. 4727–4766, 2004.

Nomenclature

b_a	Tafel slope of anode methanol oxidation reaction
b_c	Tafel slope of cathode oxygen reduction reaction
D	diffusion coefficient
d_b	bubble diameter
d_p	backing layer pore size
ΔE	thermodynamic equilibrium potential
F	Faraday constant
g	gravitational acceleration
Δg	Gibbs free energy change per mole of fuel
Δh	enthalpy change per mole of fuel
Δh_{lg}	latent heat of evaporation
I	operating current density
$I_{A,\mathrm{lim}}$	anode mass-transport limiting current density
$I_{c,oc}$	crossover current at open circuit
$I_{o,a}$	anode exchange current density
$I_{o,c}$	cathode exchange current density
$I_{x\,\mathrm{over}}$	methanol crossover current density
j_{air}	air molar flow rate at the inlet cathode
j_e	water evaporation flux
$j_{\mathrm{H_2O}}$	water flux
$j_{\mathrm{O_2}}$	consumption rate of oxygen
K_m	membrane hydraulic permeability
$M_{\mathrm{H_2O}}$	water molecular weight
n	number of electrons transferred for each molecule of fuel
n_d	electro-osmotic drag coefficient of water
$p_{\mathrm{H_2O}}$	water partial pressure
$p_{\mathrm{sat}}(T)$	saturation pressure
p_{total}	operating pressure
Q	heat generation rate
RH	relative humidity
Δs	entropy change per mole of fuel
T	temperature
u_b	bubble drift velocity through the liquid
V_{cell}	cell voltage
W_{act}	electric work
W_{max}	maximum possible work

Greek symbols

α	net water transport coefficient through the membrane
δ_m	membrane thickness
η	total energy efficiency
η_a	anode activation overpotential

η_{fuel}	fuel efficiency
η_{rev}	thermodynamic efficiency
η_{voltaic}	voltaic efficiency
μ	dynamic viscosity
μ_l	liquid water viscosity
θ	surface contact angle
ρ_l	liquid density
ρ_g	gas density
σ	liquid/gas interfacial tension
ξ	the stoichiometry defined at the current density of I
ξ_{cri}	critical air stoichiometry